TECHNISCHE UNIVERSITÄT WIEN
Vienna University of Technology

DIPLOMARBEIT

THE INVESTIGATION OF MICROCLIMATE VARIATION OF URBAN CANYONS IN VIENNA, AUSTRIA

ausgeführt zum Zwecke der Erlangung des akademischen Grades eines Diplom-Ingenieur

unter der Leitung von
Univ.Prof. Dipl.-Ing. Dr.techn. Ardeshir Mahdavi
E 259/3 Abteilung für Bauphysik und Bauökologie
Institut für Architekturwissenschaften

eingereicht an der
Technischen Universität Wien
Fakultät für Architektur und Raumplanung

von
Sung James Lim

Matrikelnr. 1127002

Wien, im April 2014

This page is intentionally left blank.

ABSTRACT

As urban areas continue to develop and grow, changes will occur in the landscape, buildings, roads, and other infrastructures that can affect the microclimate of these areas. These changes may ultimately develop into a phenomenon known as urban heat island (UHI); mainly believed to be caused by the change in surface properties and geometric forms. The main characteristic of UHI is warmer temperature when compared to the surrounding rural area. UHI affect urbanized areas, both big and small, and it is a growing concern for designers, planners, scientists, and residents alike; posing a challenge for proper building design and healthy living conditions.

Although past research has shown that urban geometry, such as aspect ratio or sky view factor, plays a key role, it alone cannot explain this fairly complex phenomenon. Other factors that can contribute to heat islands are the density of urban areas, sealing of urban structures, and increasing anthropogenic heat output. Even though heat islands in urban areas tend to display a typical pattern, the intensity can be quite different at each location, even in close proximity of each other. Much of this is due to the unique environmental conditions that make up an urban canyon.

This research investigates the street-level climate variations in urban canyons by monitoring and comparing site-specific conditions, and analyzes them against other empirical other data sources such as stationary weather measurements. Selected contributing factors will be explored to see how these factors can have an impact on the microclimate variations of selected study areas. Since much of the past research work tended to be in North America, this research will focus on microclimatic variation due to the unique characteristics of urban canyons in Vienna, Austria.

ACKNOWLEDGMENTS

The research work presented in this thesis is supported in part within the framework of the EU-project "*Development and application of mitigation and adaptation strategies and measures for counteracting the global urban heat islands phenomenon*," (Central Europe Program, No 3CE292P3). Parts of the text in this research were adopted from papers, written in relation to the projects, and co-authored with Professor Ardeshir Mahdavi. The views presented in the research are those of the author's and cannot be taken as indicative in any way of the position of the project sponsors or of colleagues and partners. Any remaining errors or discrepancies are similarly those of the author's alone.

First and foremost, I would like to thank my advisor Professor Ardeshir Mahdavi, for his generous support and guidance throughout my thesis work. He had spent much time supporting me, giving suggestions, and reviewing the results. I highly appreciate the time he had invested in me. Furthermore, my special thanks go to Milena Vuckovic and Kristina Kiesel, for being my mentors and for their countless hours of encouragement they had provided me throughout this process.

Above all, I would like to thank my wife, Susan, for her tireless patience during my thesis research. Without her love and support, none of this could have been possible.

for Maya & Noah

TABLE OF CONTENTS

1. INTRODUCTION

1.1 OVERVIEW

Luke Howard (as cited in T. R. Oke 1982) was one of the first to present evidence that the city's temperature is often warmer when compared to a nearby rural area. However, this phenomenon is not strictly confined to urban areas but is slowly transforming and expanding into the surrounding suburban and rural areas. As this trend is expected to continue, many cities around the world are in danger of facing the growing problems related to increased pollution; increased heat, increased energy expenditure, and decrease in human health (Gartland 2008).

Urbanization will continue to change the landscape, buildings, roads, and other infrastructures that will ultimately affect the microclimate of these areas. These changes may develop into a phenomenon known as urban heat island (UHI), an increase in air temperature due to the changes it brings to density, urban surface properties, and geometric forms. Although dense urban geometry presents one of the key factors contributing the overall increase in air temperatures (T. R Oke 1992; Lindberg et al. 2003; Giannopoulou et al. 2010), it alone cannot explain this fairly complex phenomenon. Other factors that have been suggested are the sealing of building and street surfaces, absence of vegetated areas, anthropogenic heat output, etc. (Robitu et al. 2006; Bouyer et al. 2009; Hebbert et al. 2011).

Heat islands in urban areas tend to display a typical pattern. As the surface characteristics of urban areas generally differ from rural areas, significant heating during the day can affect the energy balance of the city quite differently than its rural counterpart (T. R Oke 1992). For instance, during the summer months, the sun can heat exposed surfaces such as building envelopes and pavements, often raising their surface temperatures (T_S) 25-50°C above ambient air temperature (Gartland 2008). However, the intensity can be quite different at each location, even in close proximity of each other (Nunez and Oke 1977; Ali-Toudert 2005; Gartland 2008; Maleki et al. 2012; Orehounig et al. 2012). To further complicate the understanding of the impacts, majority of past studies of the UHI phenomenon have originated in North America and many subsequent studies refer back to the key results in these studies (Lafrance 2009).

1.2 OBJECTIVES

Oke (1982) had noted in his research that the relationship between population sizes vs. UHI intensity is quite different between Europe and North America. As past research work tended to be North America-centric, this research will be focused in Vienna, Austria which tends to have a different urban morphology.

This research will evaluate four contributing factors: sky view factor, density of area, sealing of surfaces, and anthropogenic heat output. It will explore how these factors can impact on the microclimate of five study areas in Vienna, Austria. Due to extreme variability in mobile measurements, this research will also address any statistical outliers from the monitored mobile measurements.

The results of this research suggest that the microclimate conditions at even relatively close proximity to each other can vary considerably, and that these variations may be related to certain characteristic features of the locations (e.g., sky view factor, vegetation, etc.). The finding corroborate past and ongoing research work being conducted in Vienna (Kiesel et al. 2012; Maleki et al. 2012; Mahdavi et al. 2013).

1.3 STRUCTURE

This thesis research is structured into six main sections as follows:

Section 1, this section.

Section 2 reviews key papers that examine fundamental characteristics of UHI. It explores the current thoughts and research on the phenomenon, and discusses possible recommendations for urban design planners and scientists through possible mitigation actions.

Section 3 describes the approach in the methodology underlying this research.

Section 4 includes the analytical result. This section provides critical analysis of the research data and analysis in the context of the U2O framework.

The research concludes with section 5 to discuss the summary of the result and present the conclusion. Additional supporting material can be found in the Appendices.

2. BACKGROUND AND LITERATURE REVIEW

2.1 OVERVIEW

This research was conducted in Vienna, Austria. Oke (1982) had noted that the relationship between population sizes versus UHI intensity is quite different between Europe and North America (Figure 1). The land use morphology and public transportation network differences have been suggested to be the main variables attributing to this contrast (Beatley 2000; Hirschler and Svanda 2009). As stated in the previous section, most past research work was conducted in North America, which has generally different population dynamics and building morphology; density or compactness, growth pattern, and distribution. This provides a unique opportunity to study the impact of the contributors of UHI in a typical European setting.

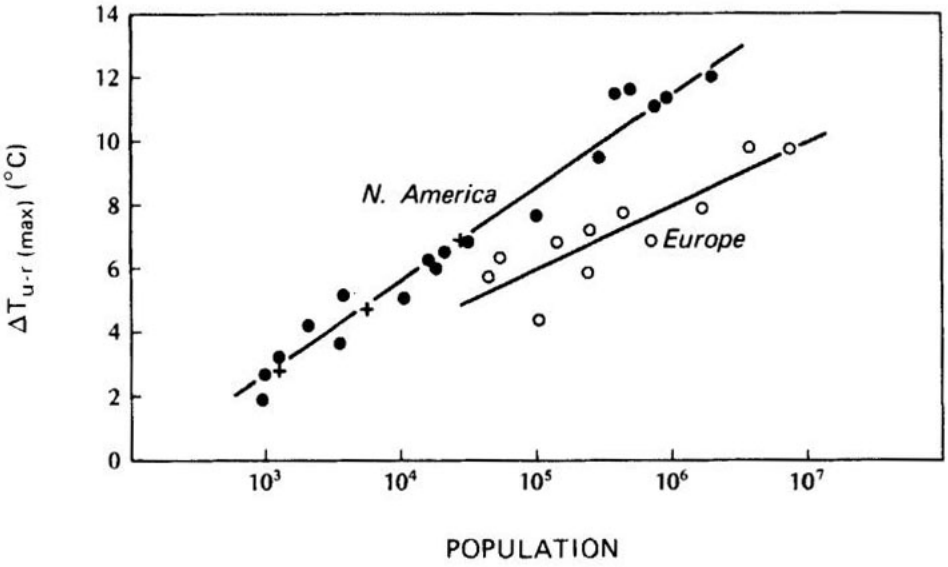

Figure 1: Relation between maximum UHI intensity ($\Delta T_{u-r(max)}$) and Population for Europe and North America settlements. Source: T. R. Oke (1982)

Vienna, the capital city of Austria, has a total area of 414.67 km^2, divided into 23 districts. Distribution of land use (Figure 2) has been roughly divided into built-up area (35.4%), green space (45.6%), bodies of water (4.6%), and roads and streets (14.4%). This data was based on information provided by Vienna City Administration - Municipal Department 23 (2012).

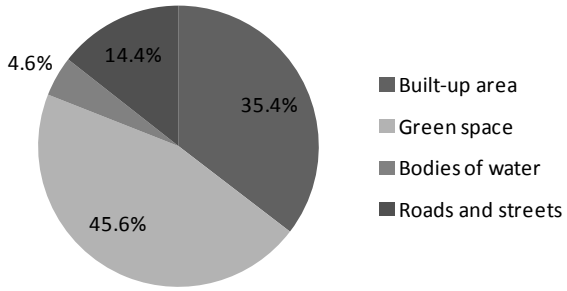

Figure 2: Distribution of land use. Source: Redrawn from figures from Vienna City Administration - Municipal Department 23 (2012).

It has had a steady population size of 1.6 million people over the last 50 years (Figure 3 and Figure 8). Despite the population stagnation, it has experienced several things during this time period; doubling of living floor space, a two and a half-fold increase in total energy consumption, a 60% rise of traffic area while the woodland and greenland areas have decreased modestly (Böhm 1998). Its population continues to shifts from rural to suburban to urban, and sometimes vice versa.

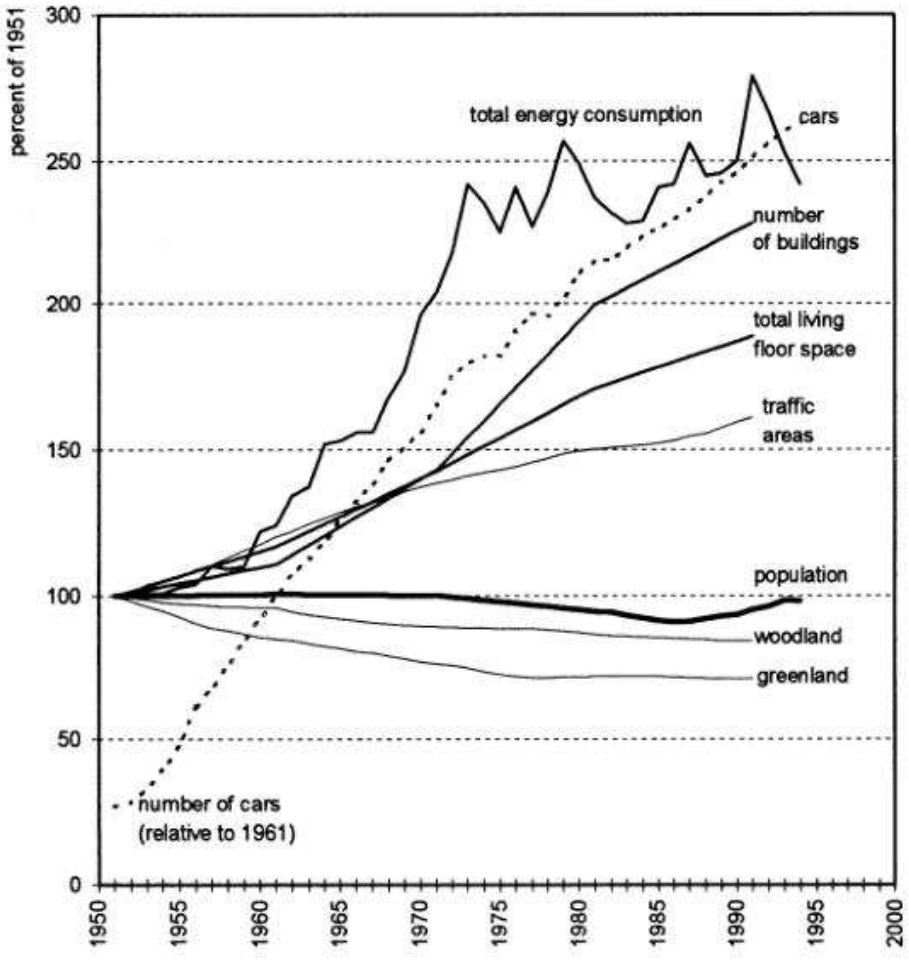

Figure 3: Urban development of Vienna since 1951. Source: "Statistical yearbooks of the City of Vienna 1951-1995," Böhm (1998)

Vienna is divided into 23 districts (Figure 4), districts 1-9 can be characterized, for the purpose of this research, as typically downtown or urban area due to its busy and crowded nature; serving as the center of culture and social activities for Vienna. These districts attract a significant share of tourists and other transient population. The residential buildings in the area tend to be of typical older Viennese style living quarters with little or no renovations (see section 2.1.3, Building Typology, for more information), and densely built. Districts 10-20 and 23 can be considered suburban. It is comprised of mainly residential areas with some mixed use. It tends to be greener and less dense than its urban counterpart. Its current population trend is increasing and the building typology of the area is predicted to change to accommodate the increase population. Finally, districts 21 and 22 can be considered suburban, bordering on rural conditions in some locations. The area tends to be greener than the other districts but at the same time some buildings tend to be of newer, and more modern building stock due to the recent population migration into the area ("Population growth in Vienna" 2009).

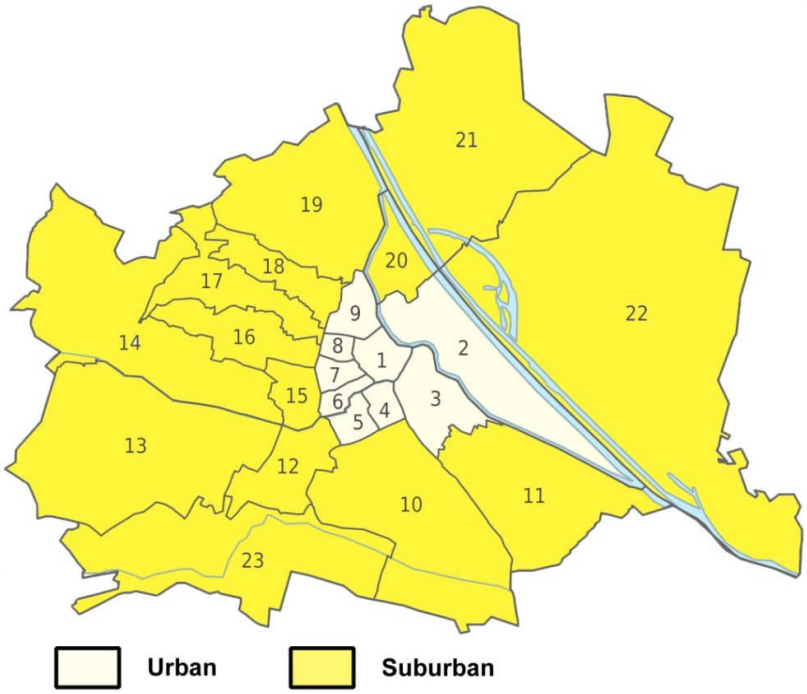

Figure 4: 23 Districts of Vienna, Austria

In this research, districts 1-9 of Vienna (cream-colored) will be referred to as "Urban," Districts 10 through 23 (yellow-colored) will be referred to as "Suburban." "Rural Weather Station" will refer to the weather station located in Seibersdorf, Austria as a basis to calculate the UHI intensity.

2.1.1 CLIMATE AND WEATHER DATA

Vienna has a rich climate dataset with a dense network of weather stations, some dating back to 1767. The dataset used as baseline conditions for this research was provided by Zentralanstalt für Meteorologie und Geodynamik (Central Institute for Meteorology and Geodynamics; ZAMG) and Stadt Wien (SW). It should be noted that Strauss et al. (2010) have found some weather stations in Austria did not pass quality test. Figure 5 provides recent analysis of the overall health of the weather stations which had improved and was found to be mostly reliable (Böhm 1998). ZAMG and SW datasets were ultimately chosen as they were considered to be quite comprehensive and relevant for purpose of the research. The datasets measured not only minimum/maximum temperature and relative humidity but also solar radiation, precipitation, and wind speed.

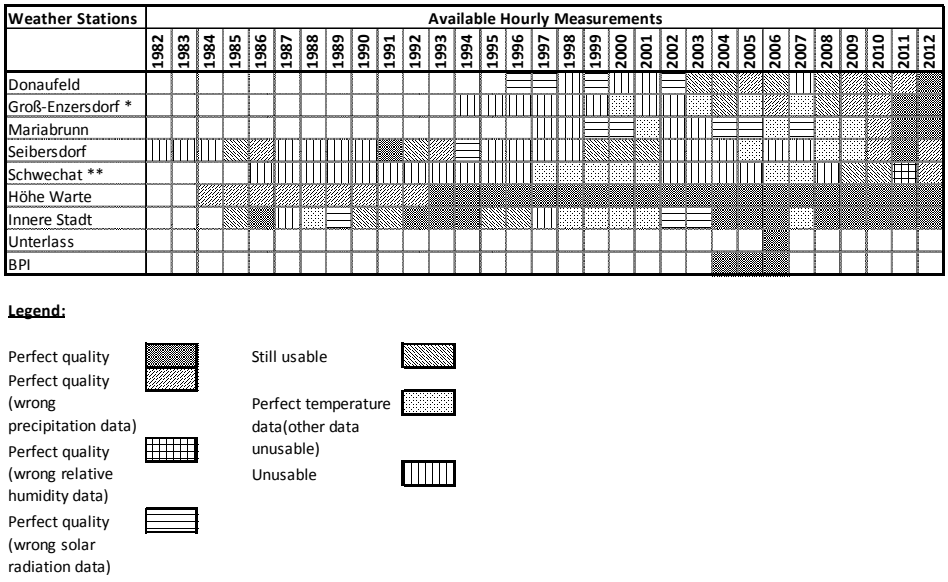

Figure 5: ZAMG monitor weather station, quality test report. Source: Böhm (1998)

2.1.2 POPULATION DYNAMICS

Urban morphology tends to a good indicator of the changing characteristics of a city as stated by Yamashita et al. (as cited in Lafrance 2009). It can be inferred, as population continues to shift from rural to suburban to urban, or sometimes vice versa, there is a tendency for change in the overall energy balance despite no significant change in population growth, such as in the case of Vienna during the past 50 years. This can be attributed to not only the change in the anthropogenic heat output, caused by increase car ownership and roadways, but by the change in the physical characteristics of the surrounding buildings due to urbanization (i.e. building surfaces, density

of buildings, loss of natural green space, height and width of streets, etc.) (Böhm 1998).

Basic concepts of population morphology in Vienna was presented by Hirschler and Svanda (2009) during the 45th ISOCARP Congress 2009. They concluded that the main driving force for the growth of the city was due to the development of better transportation network. Further suggesting that the size of the city tends to grow in direct relation to the distance a person can travel in half an hour; from 2.5km radius in 1870 to 15km in 2000 (Figure 6). This made possible for people to move further out from the city center and also for the city to bring tourists and transient populations inward.

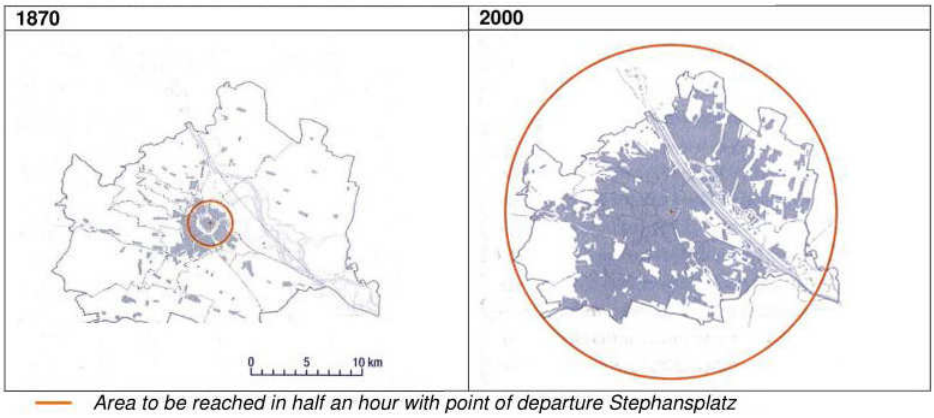

Figure 6: Development phases of mobility in Vienna 1870 and 2000. Source: Bekesi, Sandor (as cited in Hirschler and Svanda 2009)

With increased mobility, the rural area of Vienna saw the biggest growth in permanent residents while the other areas generally experienced a negative or stagnant growth during the same timeframe (Figure 7). Even as the population shifts from one area to the other, the density of the overall Vienna's population remained relatively steady during this timeframe.

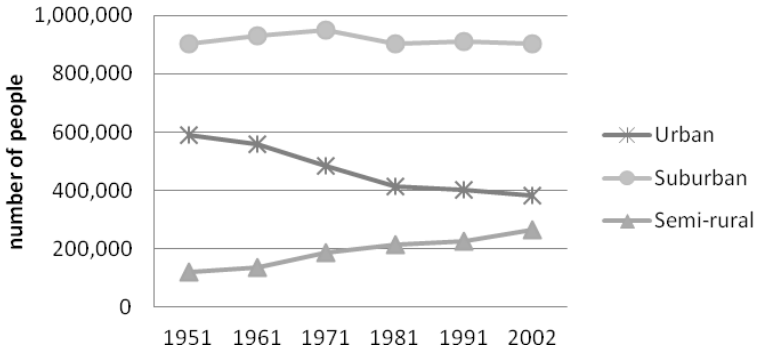

Figure 7: Residential population trend. According to "Population growth in Vienna" (2009)

Based on "Population forecast for Vienna 2011-2075" (2012), Vienna is projected to experience population growth of about 76.7% growth by 2075 (Figure 8). This figure considers mainly permanent residents of Vienna and does not factor in the tourist or transient population. To keep the research focused on evaluating the unique characteristics of the canyon conditions found in Vienna, tourist and transient population were not taken into account for anthropogenic heat production standpoint.

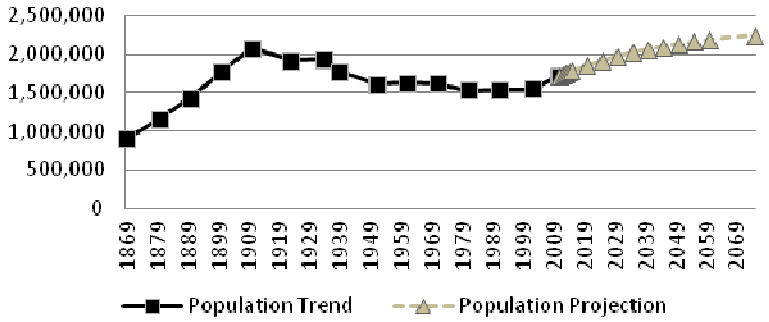

Figure 8: Residential population trend and projection. According to "Population growth in Vienna" (2009)

2.1.3 BUILDING TYPOLOGY

Building typology considered was based on *Reference buildings – The Austrian building typology* (Amtmann 2011). Two basic parameters were considered: building dimensions and construction period. This information was provided by the city of Vienna's website for Open Data ("Für eine offene Stadt - Open Government Wien" 2013). The construction period was subdivided into seven different eras (Table 13, Appendix A: Building typology); only multi-family housing was considered. The results were used to calculate approximate anthropogenic output of buildings and surface properties of buildings that compose the canyon conditions in the study.

2.2 MICROCLIMATE

To help simplify the complexity of the city-atmosphere system, Oke (1982) identified two separate atmospheric layers; Urban Boundary layer (UBL) and Urban Canopy Layer (UCL) (Figure 9). UBL is where the climate is affected by the presence of an urban area at its lower boundary. The other layer, UCL, occurs at the microscale level. The climate condition here is dominated by the nature of its immediate surroundings, such as building orientation, albedo, emissivity, thermal properties, wetness, etc.

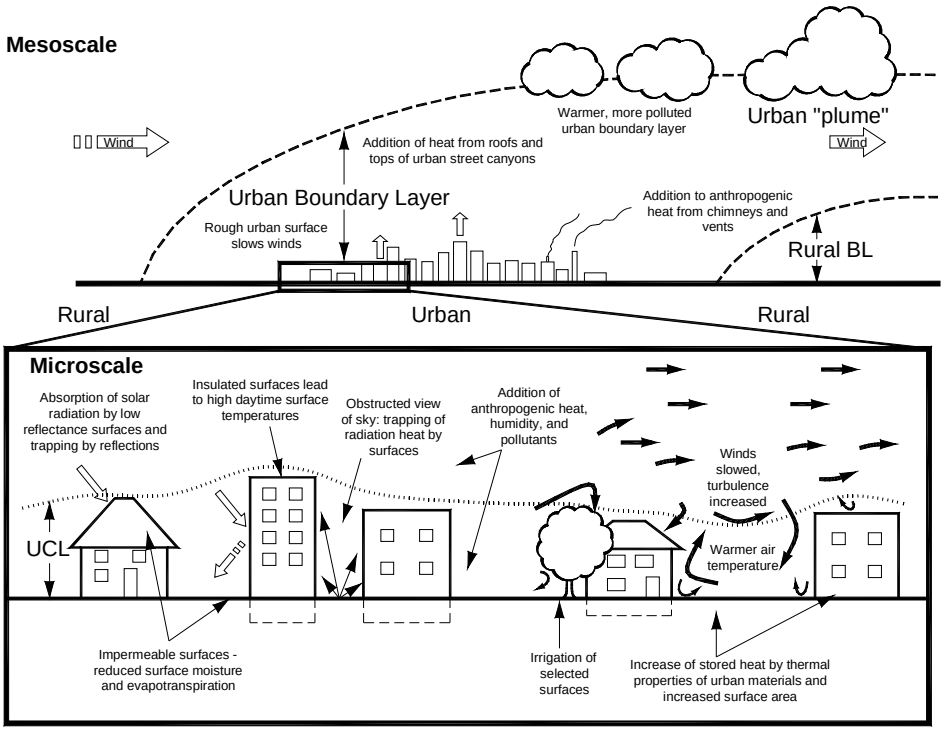

Figure 9: Two-dimensional schematic representation of the wind dynamics of the rural, urban, and microclimatic landscapes. According to T. R. Oke (1982)

Sources of urban heating within the UCL include: growing percentage of impervious surfaces, higher storage by urban structures compared with their counterpart in rural areas, increased anthropogenic heat released by substantial human activities, and presence of vegetation that may impede flow of wind (Sailor and Lu 2004; Offerle et al. 2005; Buccolieri et al. 2009).

2.3 UHI INTENSITY

Basic definition of UHI intensity is the difference in air temperature measurements made in the urban location (θ_{urban}) and immediate rural weather station location (θ_{rural}) (Tim R. Oke 1973; Kiesel et al. 2012). The formula can be summarized as the following:

Equation 1: UHI intensity. Source: Tim R. Oke (1973); Kiesel et al. (2012)

$$\Delta\theta = \theta_{urban} - \theta_{rural}$$

The atmospheric UHI usually reaches its highest intensity on summer nights, and under calm air and a cloudless sky (Oke, 1982). This is due to construction materials in an urban area exhibiting a high thermal inertia (i.e. a lower response to temperature changes), and consequently, they tend to release heat slowly after sunset and even near dawn, when most of the rural surfaces have already cooled down. On the other hand, light winds are not capable of driving turbulent exchanges of heat due to wind sheltering by buildings (Nunez and Oke 1977), while clear

skies enhance rural cooling by allowing radiative heat loss to the relatively cooler night sky. The UHI measured at the UCL may exhibit high spatial and temporal variation as a result of the variable thermal properties of the urban construction materials (Mahdavi et al. 2013). In contrast, the UHI measured at the UBL may remain relatively stable throughout day and night, since the atmosphere is less influenced by the city structure (T. R Oke 1992).

The main purpose of calculating the UHI intensity is to establish the baseline condition in which to quantify the results of any mitigation actions. Some have suggested that mitigation actions include increasing the porosity of city surface, adding vegetation, and green roof can have an long-term effect on improving the microclimate (Spangenberg et al. 2008). UHI intensity will differ depending on where the measurements are taken from. This is due to the unique characteristics of the area such as development, growth, intensity, and spatial pattern of the area (Mahdavi et al. 2013), possibly creating its own microclimate.

2.4 URBAN UNIT OF OBSERVATION (U2O)

Several past research work have indicated that the height-to-width ratio (H/W) or the sky view factor (SVF) alone is not adequate to represent the complex thermal phenomenon in the urban canyons (Eliasson 1996). UHI intensity may not be influenced necessarily by the number of inhabitants, but by other factors such as the increased sealing of urbanized surfaces and reducing evaporative elements in the city, the density of collective buildings in an area, and the increased release of the anthropogenic heat (Böhm 1998; Giannopoulou et al. 2010; Mahdavi et al. 2013).

A method to classify the unique physical characteristics of an area is an important step to effectively quantify each contributing factors of UHI. There are several past research papers that addressed this vital missing link (Deb and Ramachandraiah 2011; Stewart and Oke 2012; Mahdavi et al. 2013). This research will analyze four of the most prominent contributing factors: urban geometry, urban sealing, urban density, and anthropogenic heat output as set forth by the U2O framework (Mahdavi et al. 2013). The basis of the framework is to ascertain the specific characteristic features of an area in the context of their geometry, massing, or other physical aspects in context of contributing factors of UHI.

2.5 CONTRIBUTING FACTORS OF UHI

It would be overly simplistic to state that with increased temperature, UHI phenomenon will be more prevalent. While it can be argued that with higher ambient air temperature, the ever-expanding urban environmental influences will continue to use more energy, releasing more heat into the air; it is a complex phenomenon with even more complex causative factors (T. R. Oke 1982). This is a vicious cycle that will continue to worsen as more and more areas around the world expand their urban areas.

Some of the generally accepted contributing factors for the UHI phenomenon are associated with:

- urban geometry expressed as sky view factor,
- urban sealing expressed as impervious surface fraction,
- urban density expressed as mean building compactness,
- and anthropogenic heat output

The figure below (Figure 10), produced by the U.S. Environmental Protection Agency (EPA), gives a general idea how day and night air temperatures can differ throughout the different types of land cover. Heat is the highest both in day and night conditions over the downtown urban center. Suburban land cover also experiences extensive heat conditions during the day, but tends to cools off at night. Rural landscapes show the natural temperature trend, shown by the typically lower air and surface temperature. However, this relationship is not yet clear.

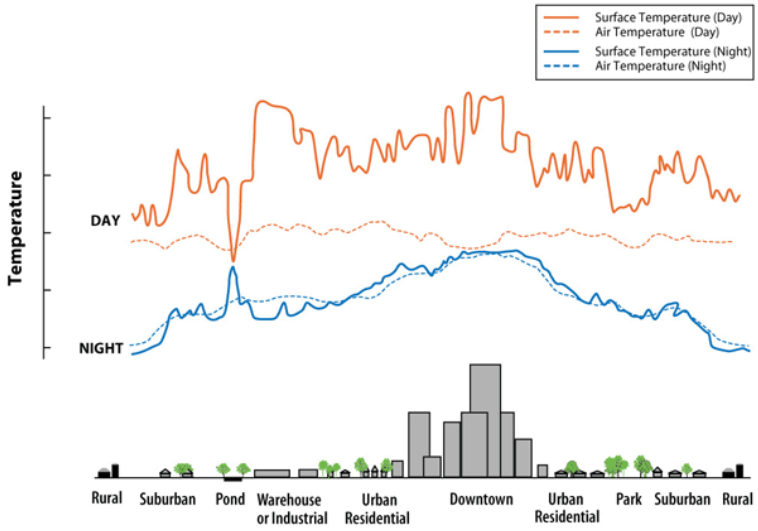

Figure 10: Diurnal surface and air temperature variance over different land use areas. Source: "Reducing Urban Heat Islands: Compendium of Strategies" (2013)

2.5.1 URBAN GEOMETRY, SKY VIEW FACTOR

Past research studies have indicated urban geometry to be the most decisive features affecting the microclimate of the urban street canyon (T. R. Oke 1982; Eliasson 1996). T. R. Oke (1982) had also noted that during clear calm weather conditions and in the absence of significant anthropogenic heat, the UHI is most related to the canyon geometry and in particular to the sky view factor.

Sky view factor (SVF or ψ_s) represents the fraction of visible sky on a hemisphere over an analyzed location (Glenn T. Johnson and Watson 1984; Holmer 1992; T. R Oke 1992). SVF is often used to describe the urban geometry of an area in context of any obstructions. Currently, there are two quite different working definitions of SVF; geometric definition (Zhang et al. 2012) and cosine-weighted definition as defined by Glenn T. Johnson and Watson (1984) (Figure 11). The former is generally suitable for human perception while the latter put more emphasis on radiation exchange between the urban surface and the sky.

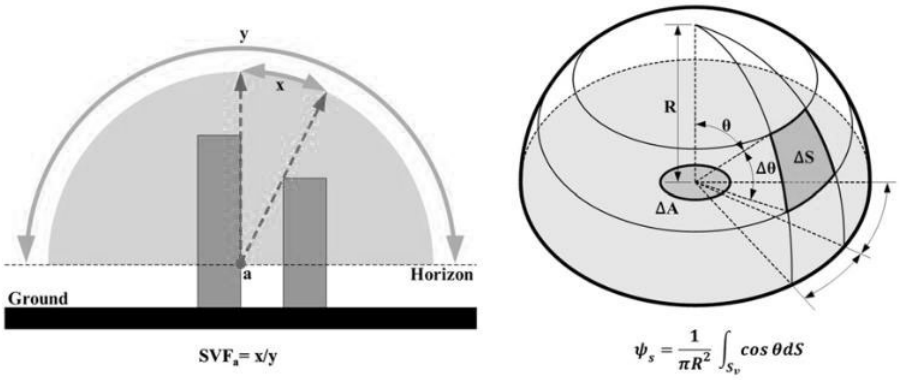

Figure 11: The geometric definition (left) and cosine-weighted (right) definition of Sky View Factor. Source: Zhang et al. (2012)

Calculating SVF can be performed by utilizing high resolution raster Digital Elevation Model (DEM) (Ratti and Richens 1999; Gál et al. 2008; Hammerberg 2014). This shadow casting algorithm utilized extensive database of individual building footprints and aerial photographs to determine individual building heights. This method provided a quick and accurate approximation of the SVF for the studied area.

2.5.2 URBAN SEALING, IMPERVIOUS SURFACE FRACTION

Rural and suburban areas continue to have their natural surface replaced by built surfaces, a process known as urbanization. This is thought to be the main cause of UHI (Akbari et al. 2001; Alexandri and Jones 2006). Natural surfaces of these areas are often composed of vegetation and moisture-trapping soils. Therefore, they release a

relatively large proportion of the absorbed radiation through the evapotranspiration process; release water vapor that contributes to cool the air in their vicinity (T. R Oke 1992). The evaporation from urban areas is decreased because of less permeable materials and less vegetation compared to their rural counterparts. As a result, cities tend to absorb a significant proportion of the incident radiation, which is later released as heat.

2.5.3 URBAN DENSITY, MEAN BUILDING COMPACTNESS

The city surface is a mixture of vertical and horizontal elements that create urban canyons; this has consequences on the amount of solar radiation that is absorbed or reflected in urban areas (Figure 12). Urban canyon, in this context, can be defined as a relatively narrow street with buildings lined up continuously along both sides; this has been widely adopted as a tool to study the impact of UHI (Nunez and Oke 1977).

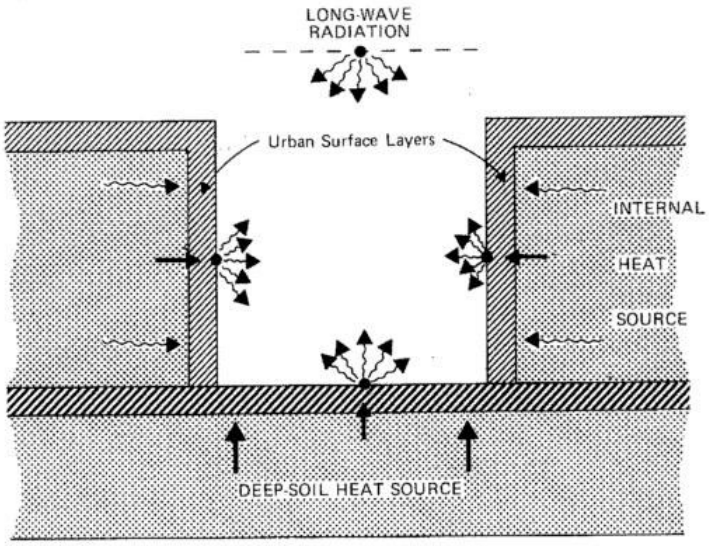

Figure 12: Schematic of the surface heat-island model with representation of the processes involved in nocturnal cooling of urban canyon surfaces under "ideal" weather conditions. Source: G. T. Johnson et al. (1991)

The dimensions of a street canyon are usually expressed by its aspect ratio, which is the height (H) of the canyon divided by its width (W); higher the aspect ratio, the taller the canyon. It has been found that the thermal storage capacity of urban environments can be influenced, to some degree, by adjusting the aspect ratio based on orientation of the urban canyon (Nunez and Oke 1977; Giannopoulou et al. 2010). The configuration and shape of the horizontal and vertical surfaces within the canyon can also have an impact on short-wave radiation being reflected onto nearby surfaces (Ali-Toudert and Mayer 2006a). The narrow arrangements of buildings along the city's streets are believed to inhibit the escape of the reflected radiation from its urban canyon. This

radiation is ultimately absorbed by the building walls (i.e. reduced sky view factor), thus increasing the urban heat release. Deeper canyons tend to decrease wind speeds and depending on the orientation increase reflective surfaces which traps heat, which due to the decreased wind speeds cannot be dissipated (Ali-Toudert and Mayer 2006b; Giannopoulou et al. 2010).

Dense urban geometry presents one of the key factors contributing to the overall increase in air temperatures (Oke 1992, Lindberg et al. 2003, Giannopoulou et al. 2010). Advection, or rate of change of an atmospheric property caused by the horizontal movement of air, can be strongly influences by compact urban development or even by presence of dense arrangement of trees.

2.5.4 ANTHROPOGENIC HEAT OUTPUT

Cities or densely populated areas typically show an increase in net radiation due to higher absorption and storage of short-wave radiation. Furthermore, dense areas and surface geometries lead to multiple reflections in the urban canyons which further increase the absorption of the shortwave radiation (Ratti et al. 2004). When combined with additional heat emissions caused by transportation, industrial processes, as well as heating, and cooling in the urban structure, it can ultimately upset the energy balance of the urban canyon (T. R Oke 1992; Pigeon et al. 2007). Energy balance is the measurement of the energy flowing in and out of surfaces; it is a sophisticated way of measuring heat island effects.

The energy balance of the volume of air extending from the ground to the top of the urban canopy layer is defined by the following:

Equation 2: Energy balance equation. Source: Kiesel et al. (2012)

$$Q^* + Q_F = Q_H + Q_E + \Delta Q_S + \Delta Q_A$$

where Q^* is the net radiation at the top of the volume, Q_F gathers the anthropogenic heat releases, Q_H is the sensible heat flux, Q_E is the latent heat flux, ΔQ_S is the storage of heat by the elements of the control volume, and ΔQ_A is the heat (or equivalent latent heat) advection through the sides of the control volume (Pigeon et al. 2007). This equation is based on the first law of thermodynamics, which states that the energy in and out of any surface must be conserved.

The Earth's energy balance (Figure 13) describes the distribution of incoming solar energy through major portions of the Earth's systems. It's similar to balancing a checkbook: the sum of all components that use

solar energy must equal the amount of incoming solar radiation. A change in the characteristics of the landscape, due to urbanization, can upset this balance on a diurnal basis.

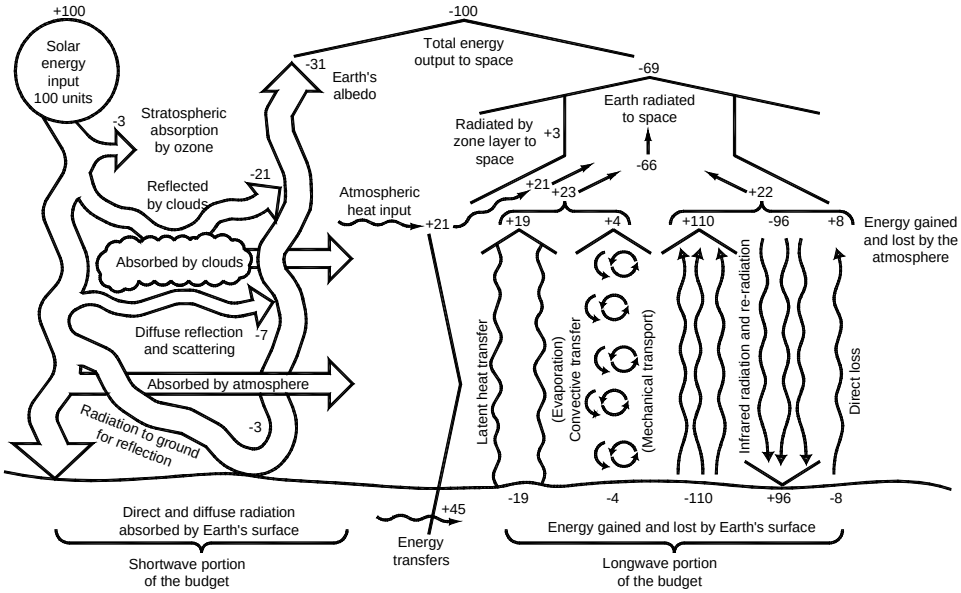

Figure 13: Energy balance of Earth. According to Christopherson (2012)

Energy interacting with Earth's surfaces comes from two sources: (1) anthropogenic or man-made, sources such as buildings, machinery and people or (2) net radiation, the amount of the sun's energy that is absorbed, not reflected or emitted away. At any moment in time, the net radiation and anthropogenic heat must be either convected away by the wind, dissipated by the evaporation of moisture or evapotranspiration from vegetation; they would otherwise be stored in the surface itself and released as longwave radiation, or as heat at a later time (Offerle et al. 2005; Quah and Roth 2012).

2.6 POSSIBLE MITIGATION ACTIONS

The frequency of urban heat islands in urbanized area is due to the greater amount of impervious material constructed throughout its landscapes. These materials tend to absorb the heat from the sun throughout the day and release it during the nighttime. Buildings, roads, pavements, etc., are typically made of water-tight or impervious construction materials. Although this particular property makes them appealing on a durability standpoint, this same property reduces the evaporation effect in the densely built city areas. There are several widely-accepted mitigation actions that is discussed in this research (Akbari et al. 2001; Sailor 2007; Gago et al. 2013); these are divided into three categories: buildings, pavements, and green area.

2.6.1 BUILDINGS

Mitigating the interaction between buildings and their immediate surroundings generally involves changing the material properties of the building envelope facing the sky and street; roof and facade. Changing the material properties of a building can be handled by applying building materials that change its solar reflectance and thermal emissivity.

Two popular choices for roofs, for instance, are cool roof (Berdahl and Bretz 1997; Akbari et al. 2001) and green roof (Alexandri and Jones 2004, 2008; Sonne 2006; Castleton et al. 2010). Cool roof rely on changing the albedo and changing its surface characteristics to raise its solar reflectance and thermal emissivity. It is generally light colored but can be of any color as longs as its surface is treated to reflect a large portion of the infrared solar radiation. While it may have a price premium over standard roof, the potential energy savings may outweigh its relatively high initial investment cost. Green roof, on the other hand, is a method in which vegetative layer covers the roof. It can be classified as extensive and intensive. Extensive green roof have a thin substrate layer with low level planting; it can be very lightweight. Intensive green roof have a deeper substrate layer to allow for deeper rooting plants, such as shrubs and trees. The former system has a reputation of low-maintenance due to the common plant type used. Thundiyil (1998) has stated that "one m^2 of grass roof can remove between 0.2 kg of airborne particulate from the air every year." Although the energy use reduction is not very large in relation to the overall building energy use, it is significant for environmental impact over the life cycle of the building (Kosareo and Ries 2007).

Recent trend in research indicated that the vertical elements of a building can be of equal importance. Cool facades show similar

mitigation benefits and characteristics as its horizontal counterpart (Doya et al. 2012). Green facades, as well, offer much of the same benefits as green roofs; reduce ambient air temperature while promoting natural cooling which reduce cooling/heating load on a building (Alexandri and Jones 2004; Olivieri et al. 2012).

2.6.2 PAVEMENTS

Majority of road surfaces are covered with asphalt. It offers a smooth surface for automobiles and is relatively cheap and easy to maintain. Its main drawback tends to be that it absorbs a large portion of solar radiation. Similar to cool roof, cool paving (Akbari et al. 2001; Gago et al. 2013) alleviates the growing cities from increase heating by sunlight. Its main benefit is that it can reduce ambient air temperature.

Another mitigation approach is to make pavement more porous. While its main virtue tends to be related to storm water management (Tennis et al. 2004), the porous surface mimic natural conditions found in rural areas. It lets the water be absorbed into the subsoil and evaporate when the pavement warms from sunlight (Saneinejad et al. 2012).

2.6.3 GREEN AREAS

A thorough research conducted in Japan (Takebayashi and Moriyama 2009) studied the benefits and characteristics of various grass native to the area. Grass had a measurable reduction in sensible heat flux. But as in the case of green roof, depending on the orientation and the vertical dimension of the canyon, the length of temporal exposure to solar radiation may be limited.

Trees contribute to the mitigation efforts by increasing shading and cooling the air by evapotranspiration of the immediate area by its leaves (Park et al. 2012). However, trees can alter the wind pattern of an urban canyon significantly enough to allow pollutants to accumulate at a pedestrian level (Buccolieri et al. 2009). The reduced turbulence it introduces in the urban canyon may negate some of those gains for. The turbulent heat transport from within streets is decreased by a reduction of wind speed (Fahmy et al. 2011). Ali-Toudert and Mayer (2007) had also found that trees, in particular, can block wind in their research. Spangenberg et al. (2008) found that deciduous tree, for example, may reduce wind speeds by up to 30-40%. Trees with large canopies will also reduce nocturnal cooling as they block some of the net outgoing long-wave radiation. Without a doubt, it is a good idea to plant trees, but it is more important to make sure to choose the type that emits low VOCs and is appropriately planted for the locale.

3. METHODOLOGY

3.1 OVERVIEW

The research investigates the intra-city microclimatic variations in several locations in the city of Vienna, Austria (Figure 14). The five selected locations were: Innere Stadt (area A), Gaudenzdorf (area B), Vienna General Hospital (AKH; area C), Höhewarte (area D), and Donaufeld (area E). These locations effectively portray urban and suburban climatic conditions in regard to the microclimatic implications of the changes in the built environment.

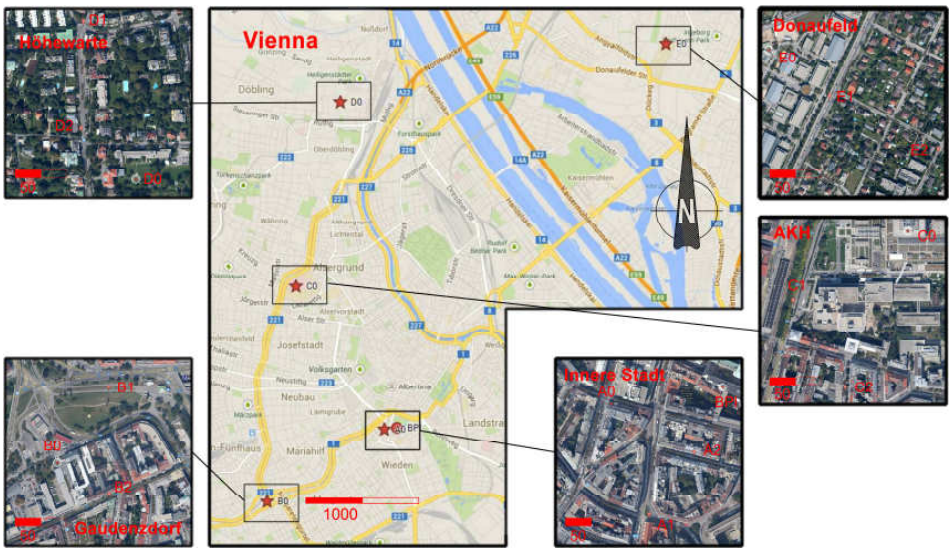

Figure 14: Area map of five study areas with two spot locations for each area.

Each study area will be monitored by one stationary and two mobile weather stations. These weather stations were monitored for two one-week periods: one week in May (spring) and one week in June (summer) 2013. Each measurement session lasted a total of four hours, once in the morning and once in the afternoon, allowing for two distinctive microclimate patterns to be captured for each location per day.

Given the uncertainty of mobile measurements, three methods were utilized in order to remove statistical outliers. The final dataset will provide the basis for microclimate and UHI intensity analysis for each location. A rural location, Seibersdorf, would serve as baseline rural condition for UHI intensity calculation. In addition, four selected influencing factors will be discussed in their possible role in influencing the UHI intensity.

For the purpose of analyzing the variation of the urban microclimate, both May and June measurements will be combined to study the systematic difference of mobile and stationary air temperature data.

3.2 INVESTIGATED AREAS

The selected five areas represent different zones with varying geometries and local conditions. To capture the specific characteristics of each area, two locations for mobile and one stationary weather station were selected (see Figure 14). Selected spot locations were positioned to capture the variety of microclimate conditions in terms of air temperature, relative humidity, wind velocity, etc. Within each area, spot location 0 represents the stationary weather stations, whereas mobile monitoring units were positioned in spot locations 1 (open field) and 2 (urban canyon).

Data from the stationary and mobile weather stations was monitored for these five study areas. The stationary weather stations are operated by the *Central Institute for Meteorology and Geodynamics* (ZAMG) and the *City of Vienna, Municipal Department of Environmental Protection Agency* (SW). Mobile weather station equipment was provided by the *Department of Building Physics and Building Ecology, Vienna University of Technology* (TU). In case of location Innere Stadt (area A), TU provided an additional stationary weather station (BPI) located above the urban canopy. The Urban Canopy Layer (UCL) is defined as the volume of air below the tops of buildings and trees as previously discussed in section 2.2.

Summary of the study areas are brief discussed, noting the physical characteristics of the stationary and mobile locations. Area A is located in Innere Stadt or center-city location; areas B and C are located in urban peripheral location; and areas D and E are in a suburban location (see Figure 4). General overview of the study area and weather station locations can be found in Figure 14.

Table 1: General overview of study areas; stationary and mobile designation

	Study area	Type	Stationary designation	Mobile designation
A	Innere Stadt	Urban (central)	A0 (ZAMG); BPI (TU)	A1, A2
B	Gaudenzdorf	Urban (peripheral)	B0 (SW)	B1, B2
C	AKH	Urban (peripheral)	C0 (SW)	C1, C2
D	Hohe Warte	Suburban	D0 (ZAMG)	D1, D2
E	Donaufeld	Suburban	E0 (ZAMG)	E1, E2

3.2.1 AREA A – INNERE STADT

This area is composed mainly of typical older Viennese style urban living quarters with little or no renovations (Figure 15 and Figure 16). The composition, geometry, and proportion of this urban streetscape are commonplace in older Viennese neighborhoods. Mobile spot A1 is located in an open plaza with few small trees and a small grassy area. Spot A2 is located in a barren street lined with cobblestone sidewalks which are generally paved with asphalt; spotty concrete patchwork in some locations, with non-existing foliage in the measurement areas. Stationary weather station (A0) is located on the roof of the *Bank Austria* building (Figure 28). Its immediate surround is similar in composition and geometry as A2. The morphological surroundings of all three weather stations (stationary and mobile) were similar.

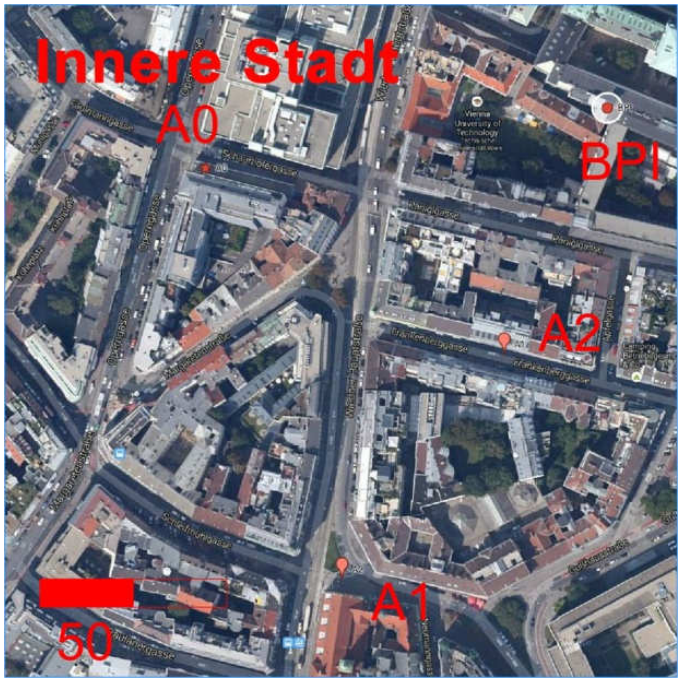

Figure 15: Locations of the measurement equipment; Innere Stadt (A0, A1, A2, and BPI)

Figure 16: Mobile weather station spot locations A1 (left); A2 (right)

3.2.2 AREA B – GAUDENZDORF

This area is composed mainly of typical older Viennese style urban living quarters with some renovations; height of buildings and density are lower than area A (Figure 17 and Figure 18). Spot B1 is located in a green-field with open access to the sky. Spot B2 is similar in composition and geometry as spot A2. Stationary weather station (B0) is located on the roof of a small one-story weather station building. The morphological surroundings of all three weather stations (stationary and mobile) were quite different.

Figure 17: Locations of the measurement equipment; Gaudenzdorf (B0, B1, and B2)

Figure 18: Location of measurement, Gaudenzdorf; B1 (left), B2 (right)

3.2.3 AREA C – AKH

This area is composed mainly of typical older Viennese style urban living quarters with some or little renovations. The streets are trees lined including some park-like areas surround AKH (Figure 19 and Figure 20). Spot C1 is located within the park-like area. The composition, geometry, and proportion of spot C2 is similar to spot A2, however with more trees. The large hospital complex in the immediate area houses the stationary weather station on the roof (C0). It is mainly made up of glass and concrete; the structure is set back from the street. The morphological surroundings of all three weather stations (stationary and mobile) were quite different.

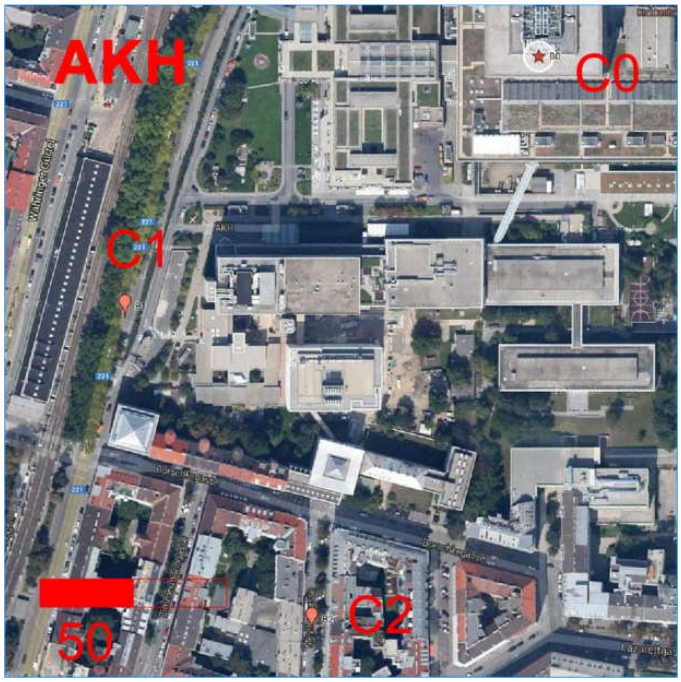

Figure 19: Locations of the measurement equipment; AKH (C0, C1, and C2)

Figure 20: Location of measurement, AKH; C1 (left), C2 (right)

3.2.4 AREA D – HÖHEWARTE

This area is composed of low- to medium-density, one- to two-story residential buildings. The composition, geometry, and proportion of this area typically found in older Viennese residential suburban neighborhood. Tree-lined streets and sidewalks are generally paved with asphalt; spotty concrete patchwork in some locations, with high-density of green areas (Figure 21 and Figure 22). Spot D1 and D2 are quite similar, except D1 is located in an open plaza. Stationary weather station (D0) is located in a green-field with open access to the sky in the ZAMG complex.

Figure 21: Locations of the measurement equipment; Höhewarte (D0, D1, and D2)

Figure 22: Höhewarte streetscape; near D1 (left), near D2 (right). Source: GoogleMaps, 2014

3.2.5 AREA E – DONAUFELD

This area is composed of low-density, single- to double-story residential buildings. The composition, geometry, and proportion of this area typically found in older Viennese residential suburban neighborhoods. Wide tree-lined streets and sidewalks are generally paved with asphalt; spotty concrete patchwork in some locations, with high-density of green areas (Figure 23 and Figure 24). Mobile spot E1 is located adjacent to the *Animal Hospital of the University of Veterinary Medicine Vienna* (AH). Spot E2 share some similarity in composition and geometry of D2. Stationary weather station (E0) is located in a brown-field with open access to the sky in the AH complex.

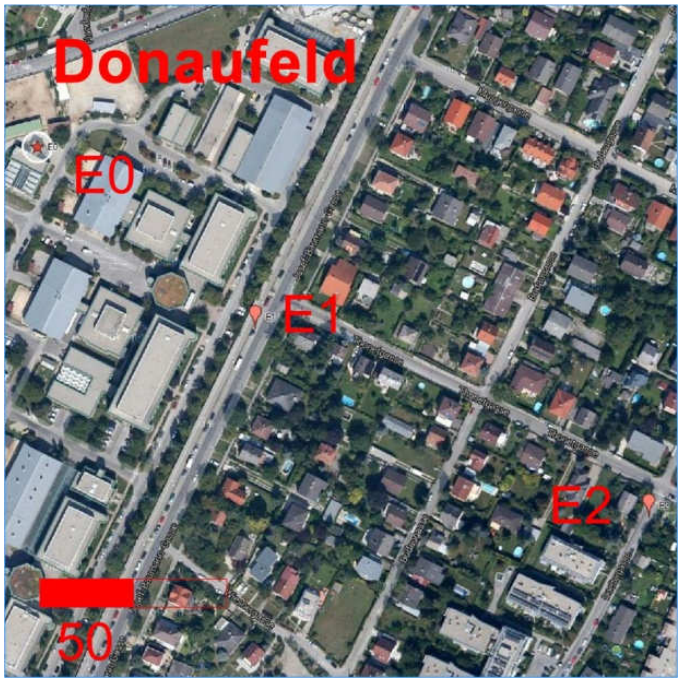

Figure 23: Locations of the measurement equipment; Donaufeld (E0, E1, and E2)

Figure 24: Location of measurement, Donaufeld; E1 (left), E2 (right)

3.3 DATA MONITOR AND WEATHER STATION INFORMATION

Microclimatic data for five areas (see Figure 14) and air temperature measurements from the stationary and mobile weather stations were monitored for these five study areas. The stationary weather stations are operated by the Central Institute for Meteorology and Geodynamics (ZAMG) and the City of Vienna, Municipal Department of Environmental Protection Agency (SW). Mobile weather station equipment was provided by the Department of Building Physics and Building Ecology, Vienna University of Technology (TU). In case of location Innere Stadt (area A), TU provided an additional stationary weather station (BPI) located above the urban canopy. The Urban Canopy Layer (UCL) is defined as the volume of air below the tops of buildings and trees, as previously discussed in section 2.2.

Summary of the study areas are brief discussed, noting the physical characteristics of the stationary and mobile locations. All five measurement locations were simultaneously monitored. Weather monitoring was conducted for two one-week periods: one week in May and one week in June 2013, twice daily. This allowed for two distinctive microclimate patterns to be captured for each location (Table 2); morning hours and afternoon hours.

Table 2: Overview of the measurement sessions for the five study areas

Date	**Time**
May 13th – 17th, 2013 (spring)	07:00 – 11:00; 17:00 – 20:00
June 10th – 14th, 2013 (summer)	07:00 – 11:00; 17:00 – 20:00

Each weather station has a different monitoring resolution. Mobile and BPI measurements were typically monitored in five-minute intervals; ZAMG data was recorded on an hourly basis; SW data was recorded on a half-hourly basis. All measurements were ultimately reduced to represent spot hourly measurements for direct comparison to each other. The ZAMG and SW maintained stationary weather stations in Vienna, in general, are considered to be a reliable source of temperature data (Böhm 1998).

3.3.1 INNERE STADT MOBILE WEATHER STATION

The mobile measurement equipments in this area are specially designed and equipped weather stations. They are mounted on two bicycles (Figure 25) and due to the nature of this setup, the measurement equipments can transverse to the monitoring site without having to be dismantled. These two mobile weather stations were identically equipped with temperature and relative humidity sensors. In addition, they were both equipped with a low power anemometer for wind speed, and a pyranometer for global solar radiation. However, A1 was only able to monitor air temperature, wind speed, and relative humidity while A2 was able to monitor all the aforementioned criteria plus global radiation measurement. This made it possible to monitor two spot locations simultaneously in this area; continuously monitoring for each four-hour session uninterrupted, twice daily. General capability of the measurement equipment is listed in Table 3.

Figure 25: Mobile weather stations, A1 (left) and A2 (right)

Table 3: General capability of mobile measurement equipment for area A

Item	Unit	Accuracy	height
Air Temperature	°C	±0.3K	1.5 m
Wind Speed	m/s	±0.5m/s or 3% of measurement	1.5m
Relative Humidity	%	±2%	1.5m
Global Radiation	W/m^2	±10%	1.5m

3.3.2 SAMPLE MOBILE WEATHER STATIONS

Mobile weather station for area B through E (Figure 26) was equipped with sensors that monitored temperature and relative humidity values; they were mounted at about 1.5 meters on a tripod. Due to the nature of the setup, the equipment had to be dismantled for each measurement session. However, the relative height of each piece of equipment was calibrated to have a consistent height of 1.5m above ground level before each measurement. The measuring sequence for each spot was taken on an alternating basis, switching spots every hour; 45 minutes monitoring and 15 minutes setting up. General capability of the measurement equipment is listed in Table 4.

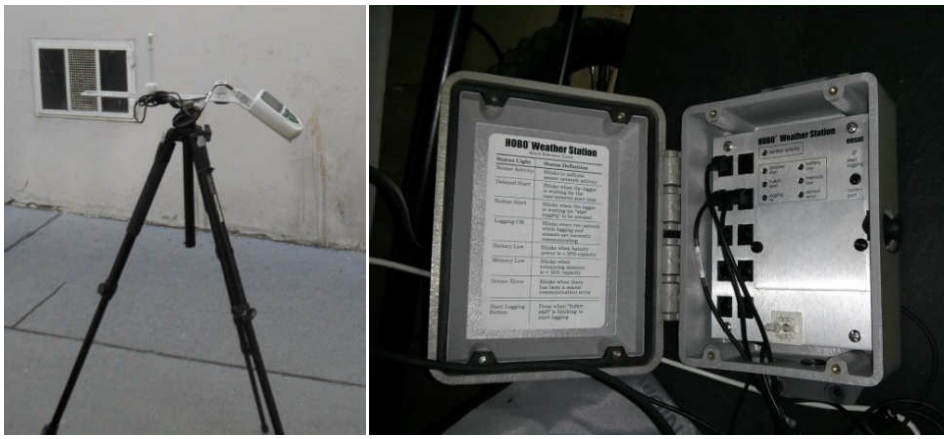

Figure 26: Mobile measurement equipment for areas B through E (left); detail of the weather station control panel (right)

Table 4: General capability of mobile measurement equipment for areas B through E

Item	Unit	Accuracy	height
Air Temperature	°C	±0.3K	1.5 m
Relative Humidity	%	±2%	1.5m

3.3.3 BPI STATIONARY WEATHER STATION

The stationary BPI weather station (Figure 27) has an array of sophisticated measurement devices. It measures the urban boundary conditions, due to the mounted heights of the measurement devices and sweeping view of the sky. General capability of the measurement equipment is listed in Table 5.

Figure 27: Roof mounted BPI weather station. Source: "Roof mounted BPI weather station" (2014)

Table 5: General capability of TU monitored weather station (BPI). Source: Lechleitner (2005)

Item	**Unit**	**Accuracy**	**height** (a.g.l., u.o.n)
Wind Direction	°	±5"	40.0m
Wind Speed	m/s	±0.5m/s or ±3% of measurement	40.0m
Relative Humidity	%	±2%	39.0m
Global Radiation	W/m^2	±10%	40.5m
Precipitation	mm		39.0m
Air Temperature	°C	±0.3K	39.0m

3.3.4 SAMPLE URBAN ZAMG MONITORED STATIONARY WEATHER STATION

Innere Stadt ZAMG monitored stationary weather station (A0) is located in the fourth district of Vienna (Figure 28). It is referred to as Innere Stadt Wetterstation ("Stationsbeschreibung & Standortsklimatologie" 2010). The weather station equipments are mounted approximately 1.66-2.3m above the lower roof of the Bank Austria building, while the wind measurement devices are mounted about 52.0m above ground level. General capability of the measurement equipment is listed in Table 6.

Figure 28: Photo of ZAMG monitored weather station, Innere Stadt. (A0). Source: "Stationsbeschreibung & Standortsklimatologie" (2010)

Table 6: General capability of ZAMG monitored urban weather station (ZAMG). Information based on "Stationsbeschreibung & Standortsklimatologie" (2010)

Item	**Unit**	**Accuracy**	**height** (a.g.l., u.o.n)
Wind Direction	°	±5"	52.0m
Wind Speed	m/s	±0.5m/s or 3% of measurement	52.0m
Relative Humidity	%	±2%	2.3m above roof level
Global Radiation	W/m^2	±10%	50.0m
Precipitation			1.66m above roof level
Air Temperature	°C	±0.3K	2.3m above roof level

3.3.5 SAMPLE SUBURBAN ZAMG MONITORED STATIONARY WEATHER STATION

This sample suburban ZAMG monitored stationary weather station is located in a brown-field in the 21st district in the AH complex located in Donaufeld (Figure 29). The weather station equipments are mounted approximately 2.0m above ground level. General capability of the measurement equipment is listed in Table 7.

Figure 29: Photo of ZAMG monitored weather station, Innere Stadt. (E0). Source: "Stationsbeschreibung & Standortsklimatologie" (2010)

Table 7: General capability of ZAMG monitored suburban weather station (ZAMG). Information based on "Stationsbeschreibung & Standortsklimatologie" (2010)

Item	**Unit**	**Accuracy**	**height** (a.g.l., u.o.n)
Wind Direction	°	±5"	2.0m
Wind Speed	m/s	±0.5m/s or 3% of measurement	2.0m
Relative Humidity	%	±2%	2.0m
Precipitation			2.0m
Air Temperature	°C	±0.3K	2.0m

3.3.6 SEIBERSDORF, RURAL LOCATION

This weather monitoring station is situated about 28.9km South of Vienna (Figure 30). This area is rural and is surrounded by farmland on the West and some dense woodland on the East. General capability of the measurement equipment is listed in Table 8).

Figure 30: Aerial view of Seibersdorf. Source: "Human footprint: Wie wir die Welt verändern" (2011)

Table 8: General capability of Rural weather station (Rural)

Item	Unit	Accuracy	height
Air Temperature	°C	±0.3K	1.5m
Wind Speed	m/s	±0.5m/s or 3% of measurement	1.5m
Relative Humidity	%	±2%	1.5m
Global Radiation	W/m^2	±10%	1.5m

3.4 MOBILE AIR TEMPERATURE MEASUREMENT QUALITY-CHECK

Given the uncertainty of mobile measurements, a thorough analysis of the monitored dataset was conducted to identify any potential outliers within the monitored measurements. Outliers are defined as any data points that are statistically inconsistent with the rest of the dataset. The inclusion of these outliers could influence the analytical outcome in an unpredictable way. However, questionable data points should never be arbitrarily discarded without proper statistical justifications. The ZAMG and SW maintained stationary weather stations in Vienna are considered to be a reliable source of temperature data (Böhm 1998), precluding any introduction of errant measurements to their respective dataset. Therefore, they did not go through quality-check, only outliers from the mobile measurements were considered for exclusion. Three statistical methods were employed in this research to remove outliers:

A. calculate the statistical upper and lower limits of the dataset (Moore et al. 2009);
B. modified Thompson's tau technique (Appendix B: Modified Thompson's tau technique and Cimbala 2011);
C. and calculate the static limits of the dataset; upper and lower, based on ΔT and Δd.

Method A, upper and lower limits of the dataset, is defined as any number outside the interquartile range, or 1.5 times the length away from difference of the first and third quartiles, can be considered an outlier. In this method all data points, mobile and stationary, were included to establish the limits for statistical purposes.

Method B, modified Thompson's tau technique, retained the upper and lower limits lines, as defined in the previous method for comparison purposes between the two methods. Only one suspected outlier was considered at a time – namely, the data point with the largest value of absolute deviation. If that data point was determined to be an outlier, it was removed and the procedure was repeated with the remaining data points until no more outliers were found. This method is further elaborated in Appendix B.

Method C, static limits, is based on the maximum hourly differences of all the respective stationary weather stations (ΔT) and maximum rate of change between adjacent temporal measurements for the five-minute interval of the BPI weather station (Δd). BPI was used for the latter criteria as it was the only weather station to provide the five-minute temporal resolution from the stationary datasets.

3.5 DATA ANALYSIS

3.5.1 AIR TEMPERATURE MEASUREMENTS ANALYSIS

The quality-checked dataset serves as a basis for the analysis of the weather station air temperature measurements. Correlation of stationary and mobile air temperature measurements are discussed and these values be compared against the regression coefficient (coefficient of termination) values to understand the trend and relationship of the measurement.

Correlation (R) and *regression* (R^2) are closely connected. The correlation is the slope of the direction and strength of the relationship between two variables x and y, giving a value between +1 and −1. The square of the correlation describes how a response variable y changes as an explanatory x changes in a simple linear regression (Moore et al. 2009). Further explanation of these terms will be discussed in Appendix C: Correlation and regression coefficient.

3.5.2 UHI INTENSITY ANALYSIS OF WEATHER STATION MEASUREMENTS VERSUS SELECTED U2O VARIABLES

The quality-checked dataset also serves as a basis for the UHI intensity analysis of the weather station air temperature measurements. Seibersdorf weather monitoring station serves as a rural basis for calculating the UHI intensity. Correlations of stationary and mobile air temperature measurements are discussed.

This dataset, consisting of one stationary and two mobile measurements for each of the five study areas is averaged to form two sets of values for each area, five in the morning and five in the afternoon; producing a total of 10 data points (Table 10). Overall values of the U2O variables for each area are presented in this portion of the research (Table 12). The relationship of these factors: urban geometry, urban sealing, density, and anthropogenic heat output, are explored to ascertain if there are differences between data obtained from standard (stationary) weather stations and those located in an urban canyon or in an open-field.

4. RESULTS AND ANALYSIS

4.1 OVERVIEW

The data points for all temperature measurements, stationary and mobile, are graphed for the months of May and June (Figure 31 and Figure 32) for analysis. Boxplot graphs present the temporal distribution of all points in the dataset (Figure 33 and Figure 34). Finally, all stationary measurements are removed from the graphs that follow (Figure 35 and Figure 36) but were nonetheless included in establishing the statistical limits. In this latter set of graphs, BPI measurement was included to illustrate the diurnal temperature trend.

Initial inspection of the daily baseline graphs in Figure 31 and Figure 32 would indicate the occurrence of some potential outliers in the datasets. However, as previously mentioned in section 3.4, it is prudent to handle the dataset with judicious application of established statistical methods for any outlier removal. The three different methods used assess the dataset are: method A – upper and lower limits; method B – modified Thompson's tau technique; and method C – static limits.

4.2 DAILY BASELINE

The graphs below (Figure 31 and Figure 32), illustrates the temporal distribution for all points in the dataset for daily temperature trend on an hourly basis.

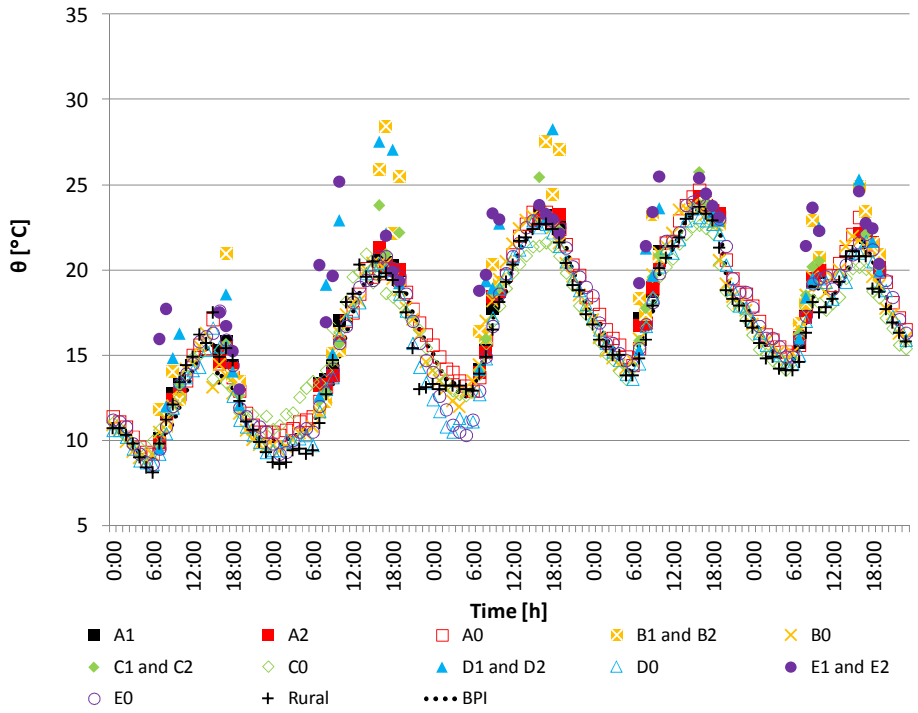

Figure 31: Daily temperature trend baseline, hourly basis; May

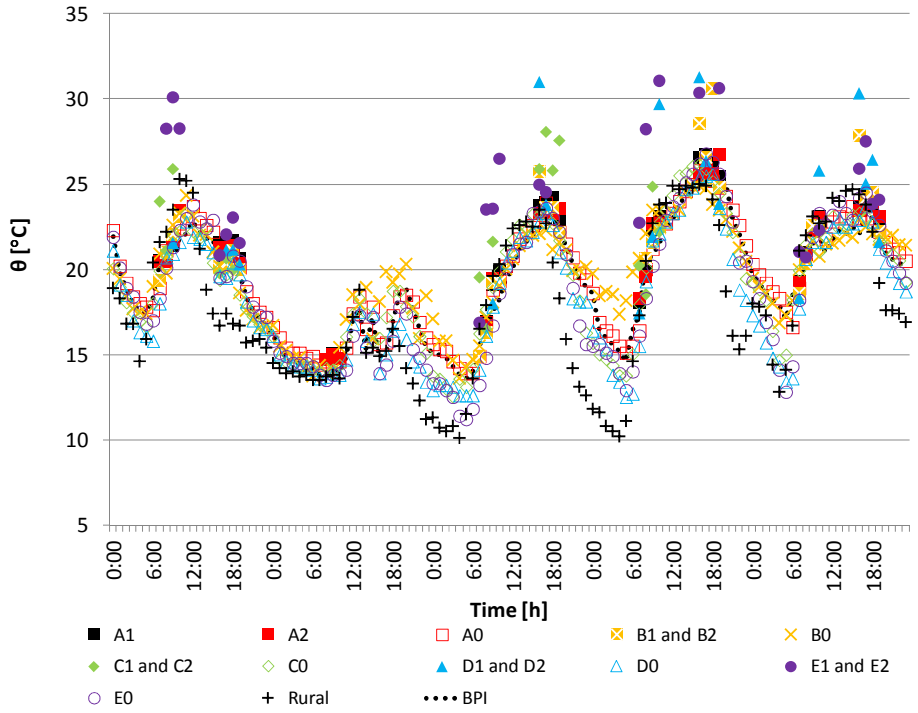

Figure 32: Daily temperature trend baseline, hourly basis; June

The boxplot graph below (Figure 33 and Figure 34) illustrates the temporal distribution for all points in the dataset; mobile and stationary. It is somewhat evident from this representation where the distribution of potential outliers might occur, but further analysis follows in order to find definite outliers.

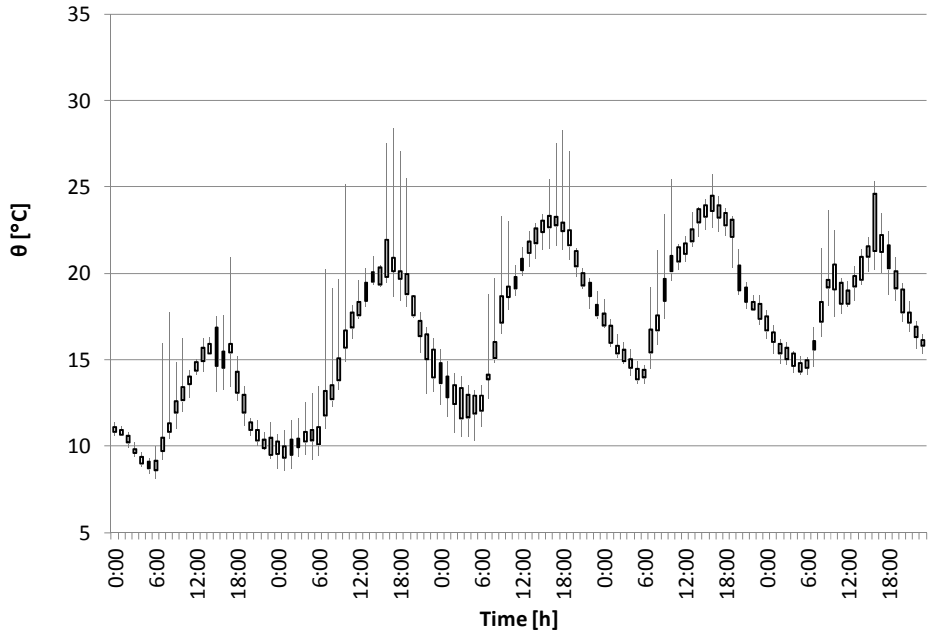

Figure 33: Boxplot of the daily temperature trend; May

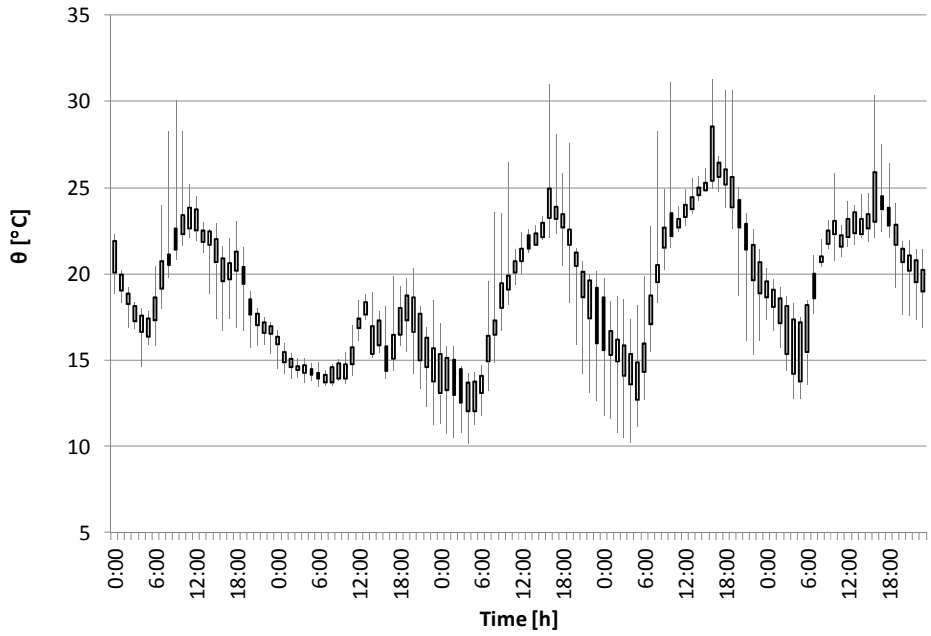

Figure 34: Boxplot of the daily temperature trend; June

4.3 MOBILE DATASET QUALITY-CHECK

In order to analyze monitored measurements for quality-check, stationary air temperatures are removed from further graphical representation, as outlined in the following graphs (Figure 35 and Figure 36); nonetheless they were still considered in calculating the statistical limits of the respective methods. BPI measurement is included to illustrate the diurnal temperature trend, for this instance.

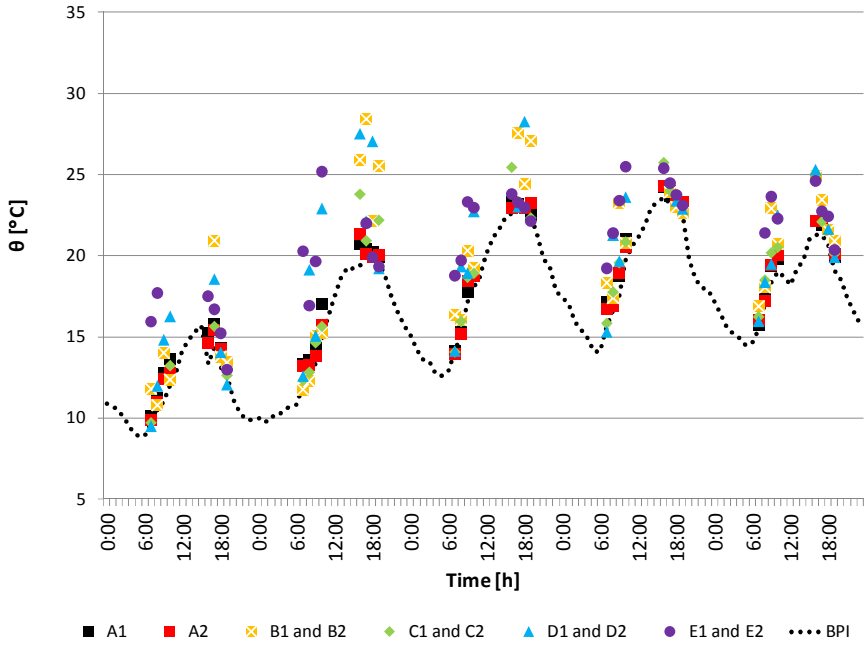

Figure 35: Diurnal temperature trend; May

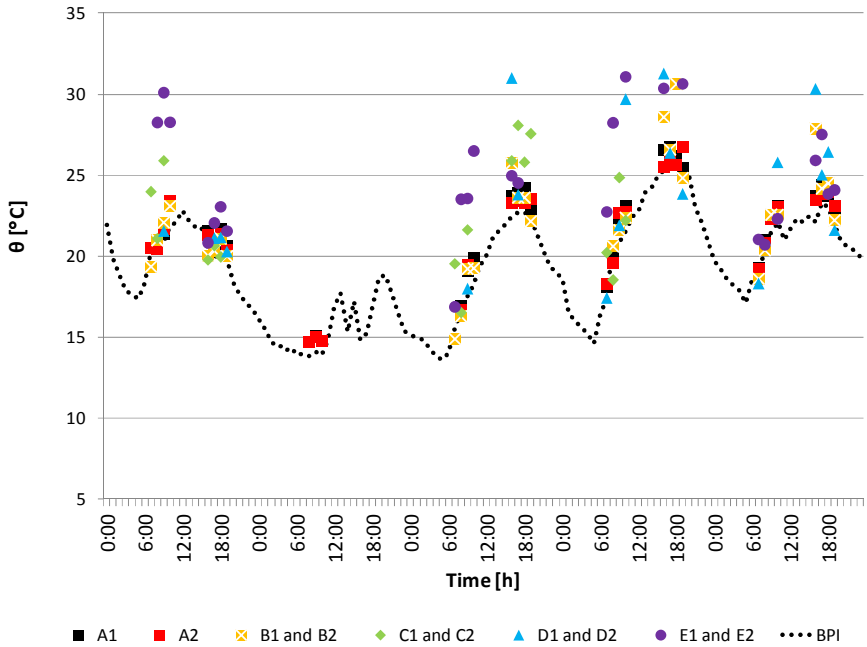

Figure 36: Diurnal temperature trend; June

4.3.1 METHOD A – UPPER AND LOWER LIMITS

A statistical method of calculating the upper and lower limits of the dataset is implemented to exclude any potential outliers. The upper and lower limits are illustrated in the graph below (Figure 37 and Figure 38) to illustrate the boundaries of these limits.

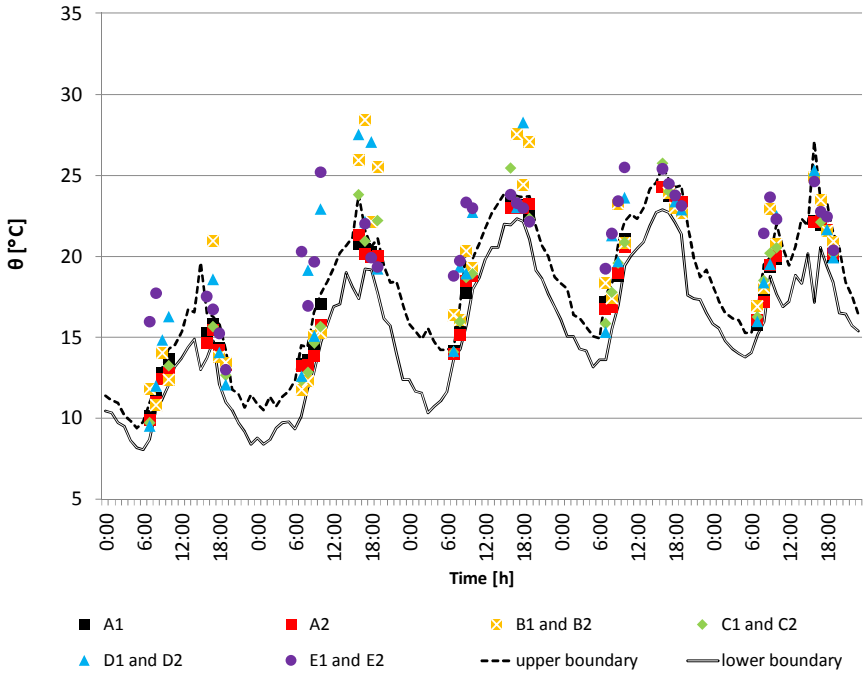

Figure 37: Statistical upper and lower limits of the daily temperature trend; May

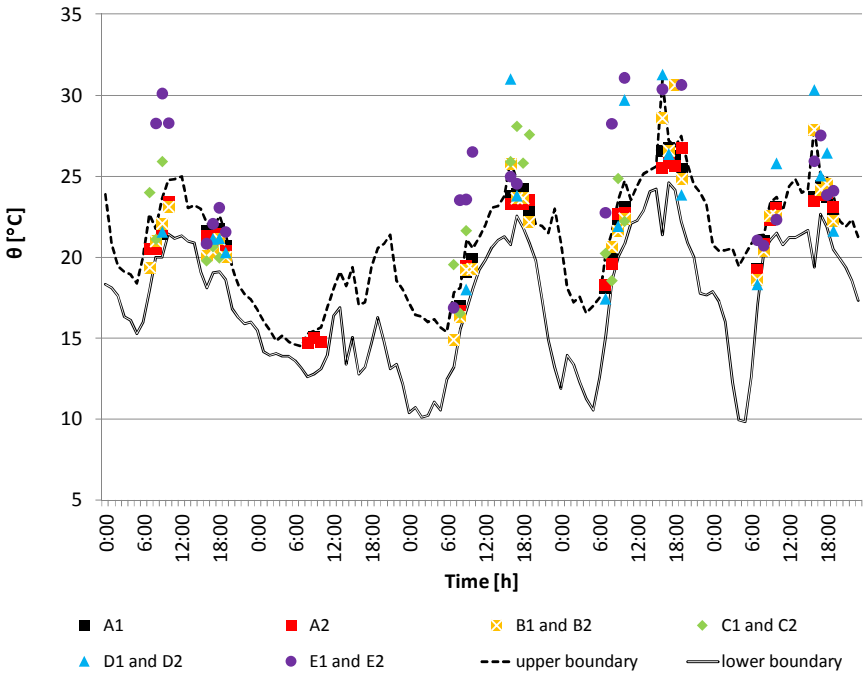

Figure 38: Statistical upper and lower limits of the daily temperature trend; June

This method provides a quick and easy approach to evaluate the data points for potential outliers. The results of the removal of the outliers are illustrated in the following graph (Figure 39 and Figure 40). Most outliers occur in the upper temperature range.

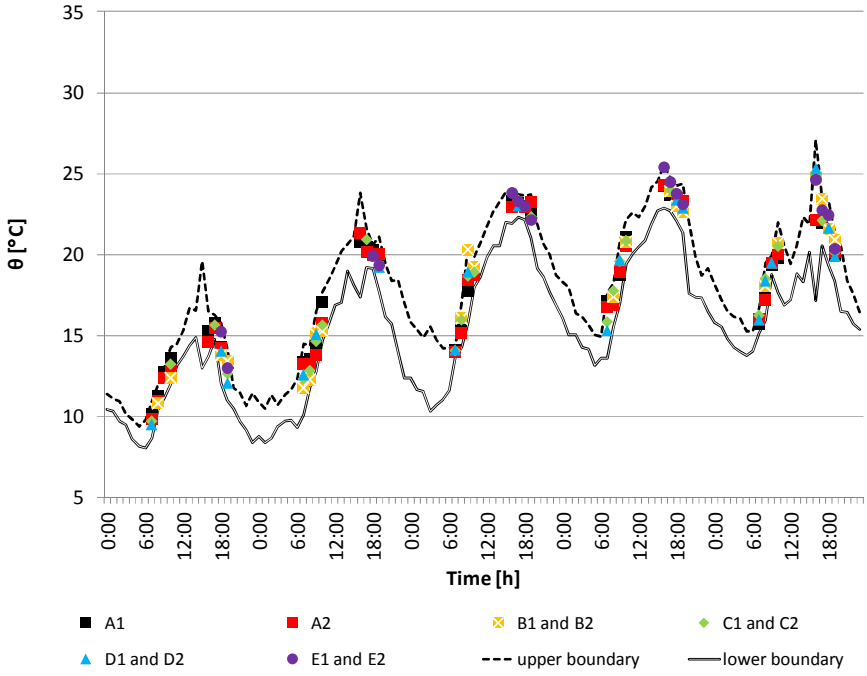

Figure 39: Statistical upper and lower limits of the daily temperature trend, removed outliers; May

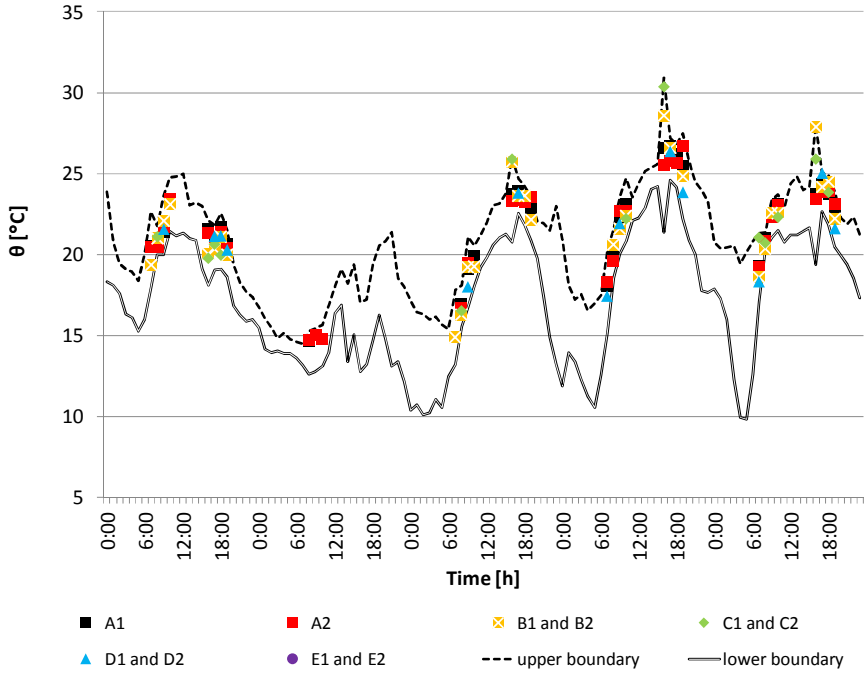

Figure 40: Statistical upper and lower limits of the daily temperature trend, removed outliers; June

4.3.2 METHOD B – MODIFIED THOMPSON'S TAU TECHNIQUE

One of the most prominent method developed to identify these outlying data points was developed by Thompson (1935); he proposed a criterion in which a portion or the observation in whole is rejected based on his method to remove any "defect" within a dataset. The Thompson tau method led to the development of a modified version aptly named modified Thompson's Tau technique (further elaborated in Appendix B: Modified Thompson's tau technique; Cimbala 2011). This method considers only one suspected outlier at a time; most suspected outlier being the data point with the largest absolute deviation value. The procedure was repeated until no further outliers are found.

The following graphs retain the upper and lower limits lines, as defined in the previous method to facilitate the comparison between the two methods, method A and B. After several iterations based on Method B application, several data points remained, which had been previously removed by Method A (see Figure 39 and Figure 40). The procedure was repeated multiple times to remove any further remaining outliers. The second iteration found one additional outlier while the final iteration did not find any further outliers in the dataset (Figure 43 and Figure 44).

As illustrated in the following graphs (Figure 41 and Figure 42), some data points remain which has been removed by the upper and lower limits method. The single iteration of the technique may have contributed to this discrepancy. The upper and lower limits lines, as defined in the previous method, are retained in the graph for clear correlation between the two methods. Additional iterations were performed to remove any further outliers.

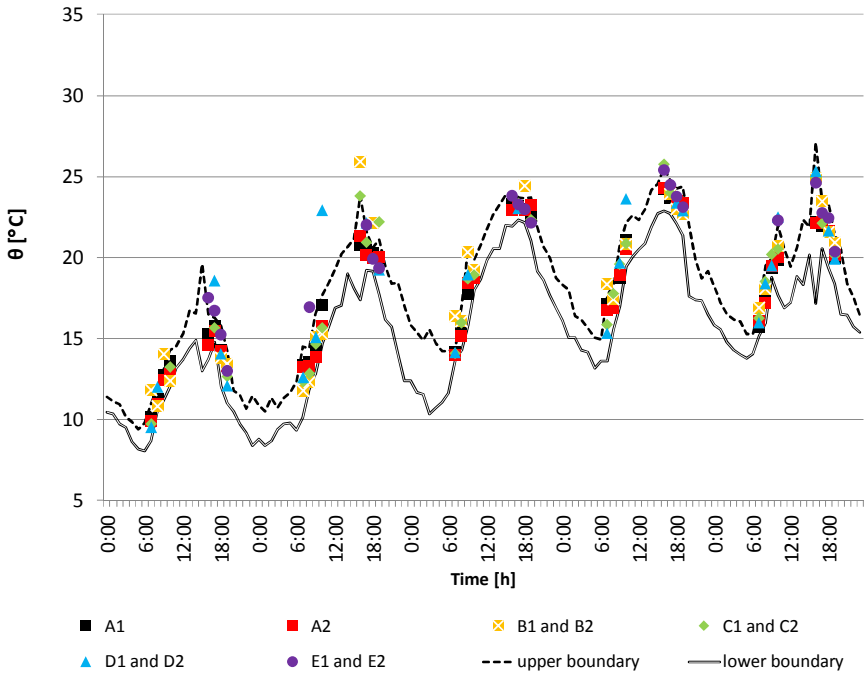

Figure 41: Modified Thompson's Tau technique, single iteration; May

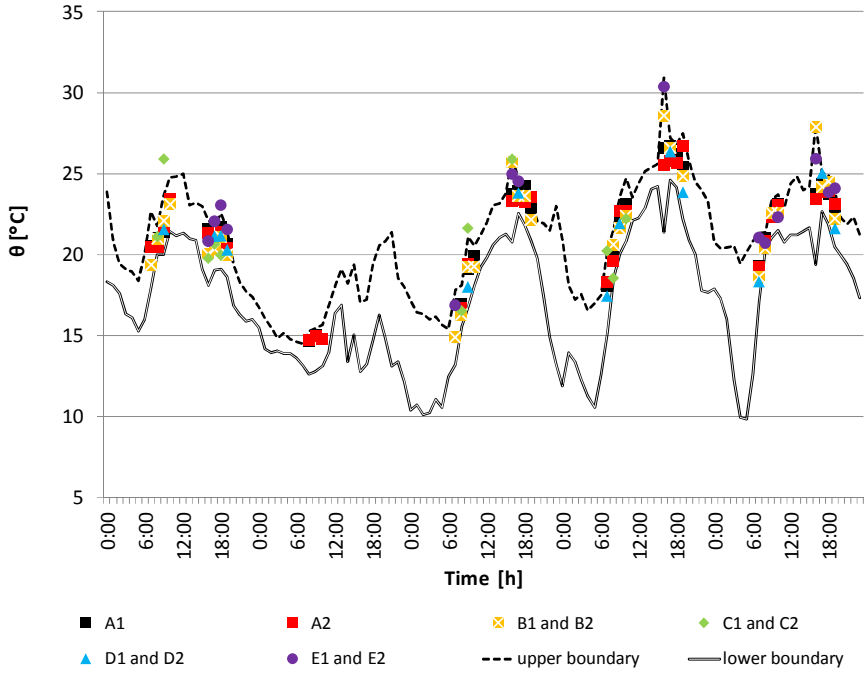

Figure 42: Modified Thompson's Tau technique, single iteration; June

The procedure was performed additional times to remove any remaining potential outliers (Figure 43 and Figure 44). Even though some data points may have initially appeared to be outliers, subsequent iteration has recognized these points as being statistically relevant and thus they are kept in the dataset.

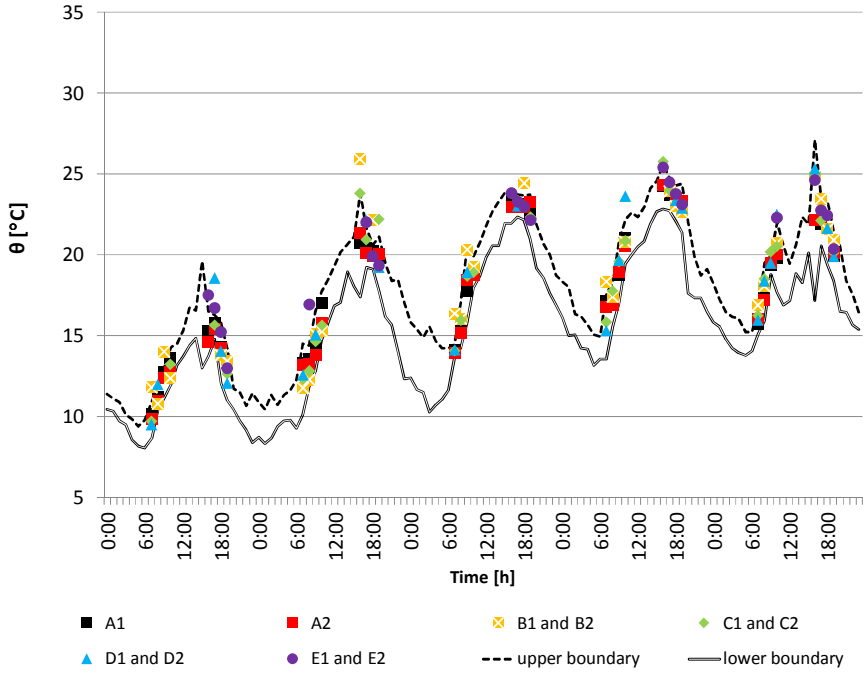

Figure 43: Modified Thompson's Tau technique, final iteration; May

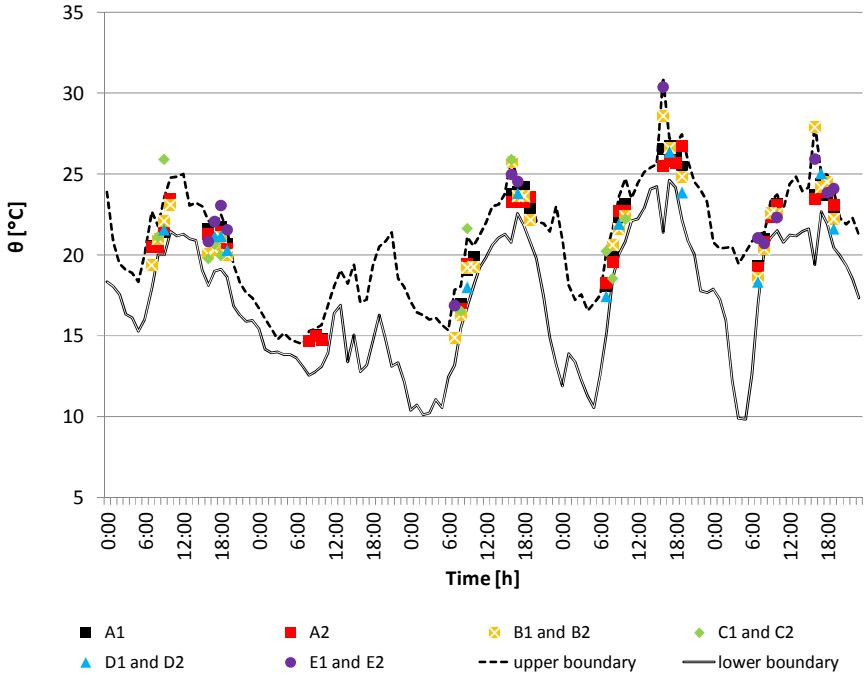

Figure 44: Modified Thompson's Tau technique, final iteration; June

4.3.3 METHOD C – STATIC LIMITS

The stationary measurement equipment in Vienna is deemed to be reliable sources for reference purposes. Static limits – method C is based on a principle that mobile measurement should not deviate more than the maximum change in temperature (ΔT) of adjacent reference stationary weather station (i.e., ZAMG, SW, BPI). In addition, for the sub-hourly measurements, the maximum value for rate of change in temperature (Δd) of the BPI weather station was calculated. BPI was the only weather station to provide the five-minute data point resolution. These two values are used in the generalized algorithm for the upper and lower limit criteria for identifying potential outliers in the dataset.

Maximum ΔT value between adjacent temporal measurements for all stationary datasets is calculated (Figure 45 and Figure 46), at an hourly basis; value was determined to be 3.17K. The greatest adjacent temperature variance for the BPI dataset was calculated to be 1.30K; for the five minute intervals. This method had identified additional outliers that were found to be out of the statistical "norm" for a given time interval.

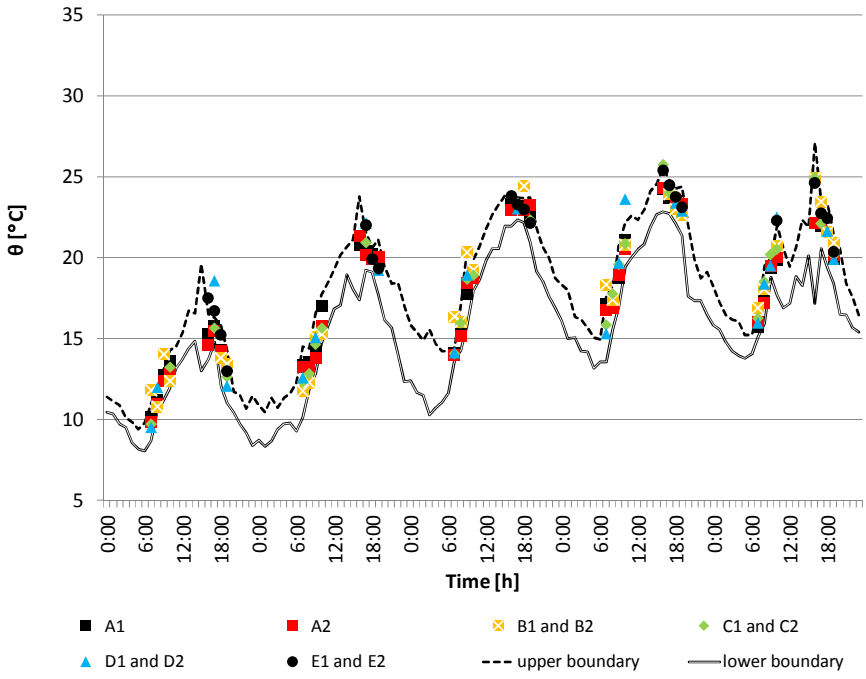

Figure 45: Static limits; May

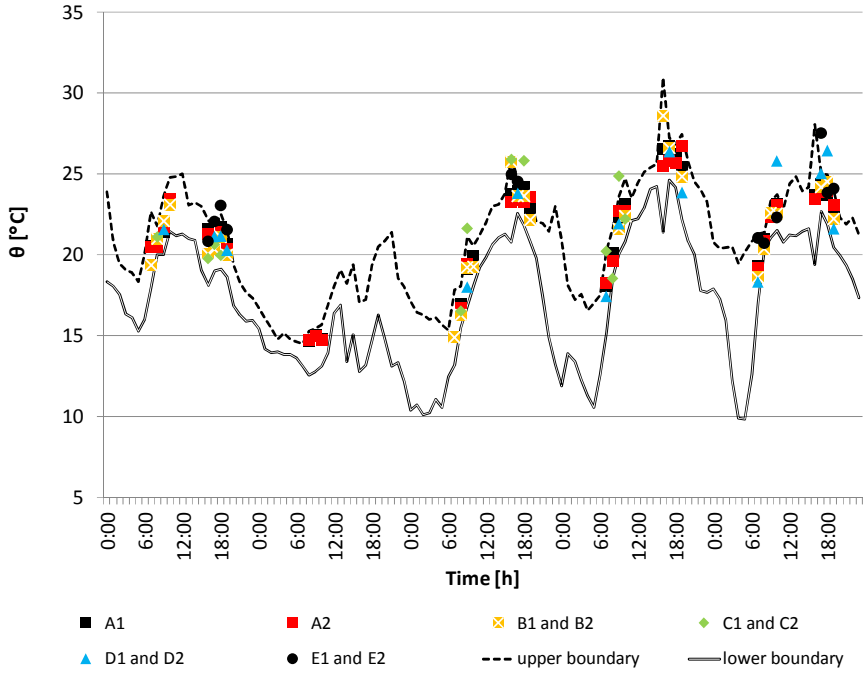

Figure 46: Static limits; June

4.3.4 SUMMARY OF FINAL DATASET

The temporal distribution of temperature for May and June as presented by the boxplot in Figure 33 and Figure 34 suggest that the potential outliers would occur mostly in the upper temperature range. Analyses of the monitored dataset were conducted to identify any potential outliers within the dataset using three statistical methods. Method A established the upper and lower statistical limits as presented in section 4.3.1. These limits were used as a basis to compare method B as presented in section 4.3.2 and method C as presented in section 4.3.3. By analyzing for and appropriately removing potential outliers, the remaining data points can be used for further analysis.

The research monitored a total of 387 hourly mobile air temperature measurements from the five study area. As displayed in the graph below (Figure 47), method B (green square and dotted line) – the modified Thompson's tau technique – removes the least number of monitored data points (328 data points remaining) while still providing statistically acceptable measurements. Therefore, the final dataset established by method B is used in the following analyses.

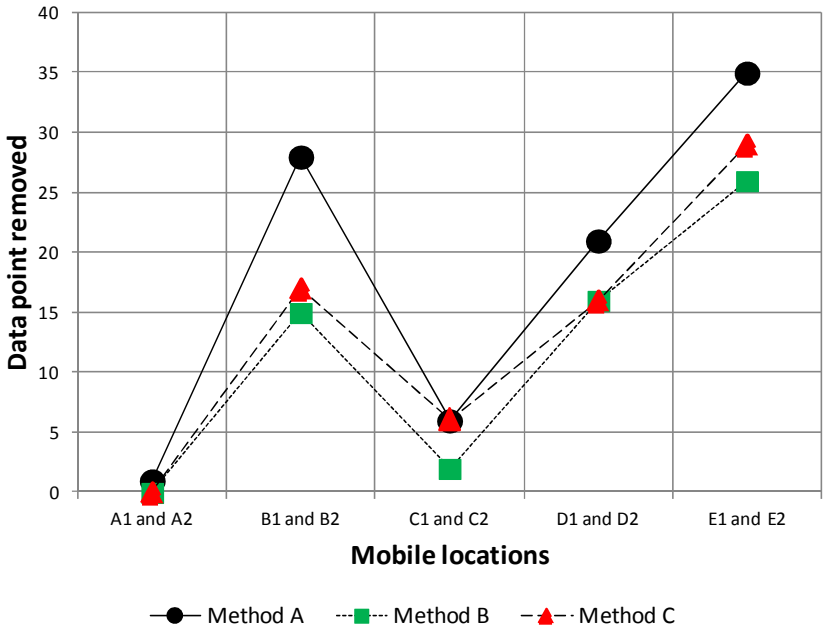

Figure 47: Number of data points removed as outliers (black circle and continuous line: Method A; green square and dotted line: Method B; red triangle and dashed line: Method C)

4.4 MICROCLIMATE ANALYSIS OF WEATHER STATIONS MEASUREMENTS

The finalized dataset, with outliers removed, serves as a basis for the following analyses of the weather station air temperature measurements. This will be referred to as “valid” or “finalized” data points.

This part of the research analyzes the air temperature measurement in two-fold contribution. First, stationary air temperature measurements are compared with simultaneously monitored data from the BPI weather station. Second, mobile versus simultaneously monitored reference stationary weather station are analyzed.

Mobile monitoring units for all five study areas were positioned in either open field (spot locations 1) or in an urban canyon (spot locations 2); stationary weather stations (spot locations 0) were generally located on top of buildings (see section 3.2 and 3.3).

In this section, there are three questions that this research attempts addresses: 1) are there any variations in the air temperature measurements due to equipment location? 2) is there a trend or regression that can be concluded from this analysis? 3) is so, what is it?

4.4.1 AIR TEMPERATURE CORRELATION – STATIONARY WEATHER STATION MEASUREMENTS VERSUS BPI WEATHER STATION

The graph below (Figure 48) compares the stationary weather station air temperature measurements (θ_S) with simultaneously monitored data from the BPI weather station (θ_{BPI}); white triangles represent stationary measurements.

The graph suggests that there is some variance with the air temperature measurements obtained from the five stationary monitoring sites. However, the regression coefficient values (R_T^2) of the five stationary weather stations (Table 9) indicate a strong relationship among the stationary weather station to the BPI weather station. ZAMG monitored stationary weather station in area A displayed the strongest correlation to BPI, possibly due to the proximity and similarity in the physical context of these two stationary weather stations.

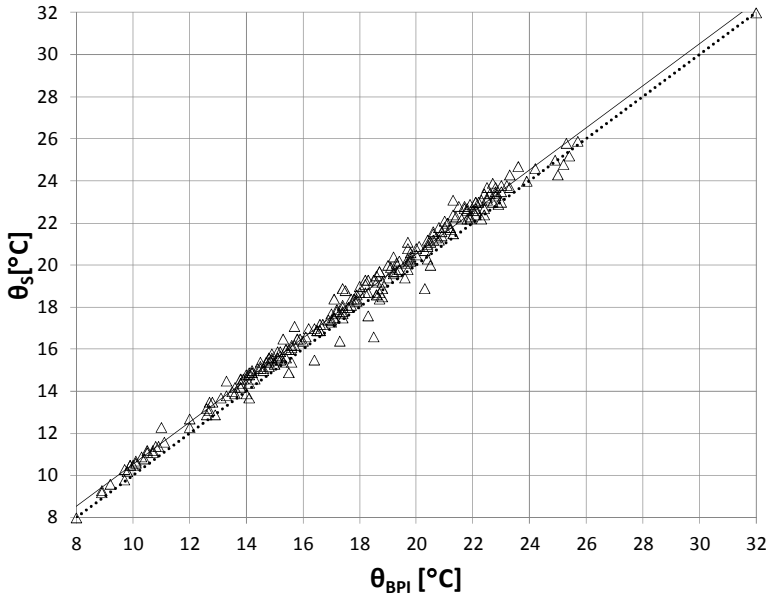

Figure 48: Stationary air temperature measurements (white triangles; continuous line represents regression coefficient line for stationary measurements) in all area versus BPI weather station (dotted line)

Table 9: Degree of agreement of the five stationary temperature measurements in all areas versus BPI measurement (dotted line, Figure 48)

Stationary spot location	R_T^2
A0	0.99
B0	0.92
C0	0.91
D0	0.92
E0	0.94

4.4.2 AIR TEMPERATURE CORRELATION – MOBILE WEATHER STATION MEASUREMENTS VERSUS STATIONARY WEATHER STATION

Figure 49 compares the measurements of the mobile weather stations air temperature measurements (θ_M) with simultaneously monitored data from the reference stationary weather stations (θ_S); white triangles represent mobile measurements.

The graph suggests that air temperature measurements obtained from the mobile monitoring stations within the urban fabric are systematically higher than stationary weather station data. This is indicated in the systematic shift of the regression coefficient line through all data (continuous line in relative to the theoretical line of perfect agreement (dotted line in Figure 49 through Figure 59).

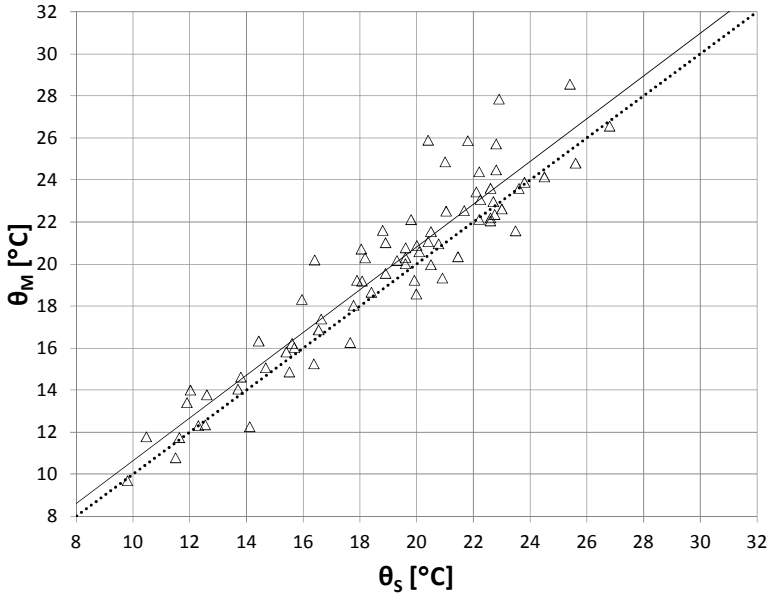

Figure 49: Mobile versus stationary temperature measurements (white triangles; continuous line represent regression coefficient line for mobile measurements in all areas versus reference stationary weather stations; dotted line: theoretical line of perfect agreement)

In order to better understand the behavior of mobile measurements in the individual study areas, Figure 50 through Figure 59 compares the 10 mobile weather station measurements (θ_M) with simultaneously monitored data from their respective stationary weather stations (θ_S).

4.4.2.1 WEATHER STATION MEASUREMENTS – AREA A

The mobile versus stationary weather station measurements for area A is graphed for analysis (Figure 50 and Figure 51). The mobile data points from these two spot locations (A1 and A2) are compared with the simultaneously monitored stationary weather station measurement in spot location A0 (diagonal dotted line in the graphs).

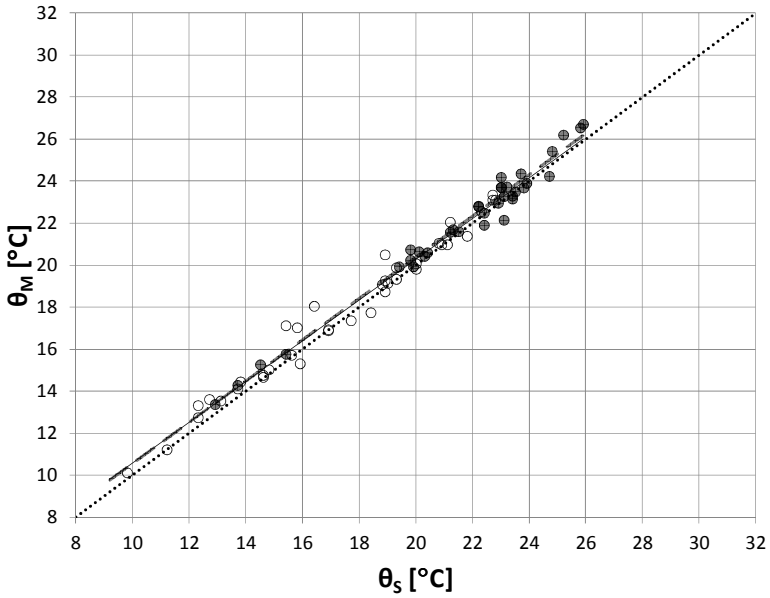

Figure 50: Mobile versus stationary air temperature measurements, mobile spot location A1 (white dots + solid regression coefficient line: morning measurements; dark dots + dashed regression coefficient line: afternoon measurements; dotted line: theoretical line of perfect agreement)

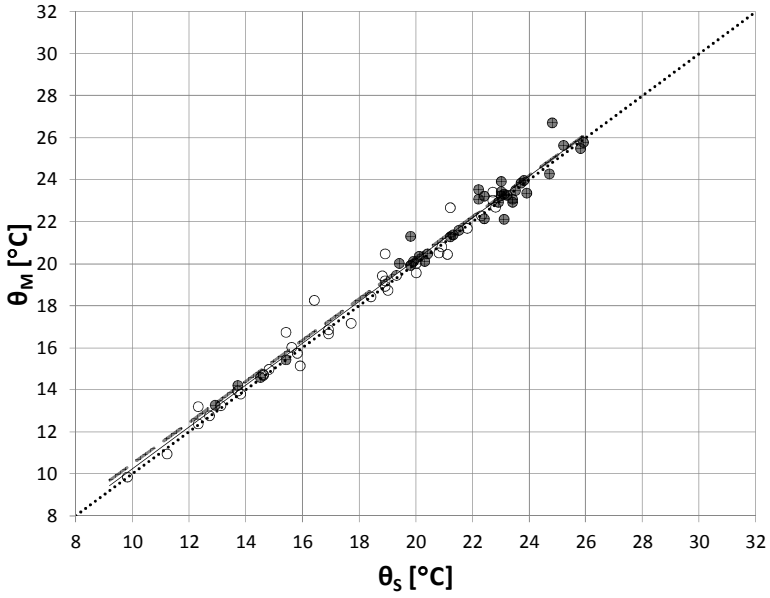

Figure 51: Mobile versus stationary air temperature measurements, mobile spot location A2 (white dots + solid regression coefficient line: morning measurements; dark dots + dashed regression coefficient line: afternoon measurements; dotted line: theoretical line of perfect agreement)

4.4.2.2 WEATHER STATION MEASUREMENTS – AREA B

The mobile versus stationary weather station measurements for area B is graphed for analysis (Figure 52 and Figure 53). The mobile data points from these two spot locations (B1 and B2) are compared with the simultaneously monitored stationary weather station measurement in spot location B0 (diagonal dotted line in the graphs).

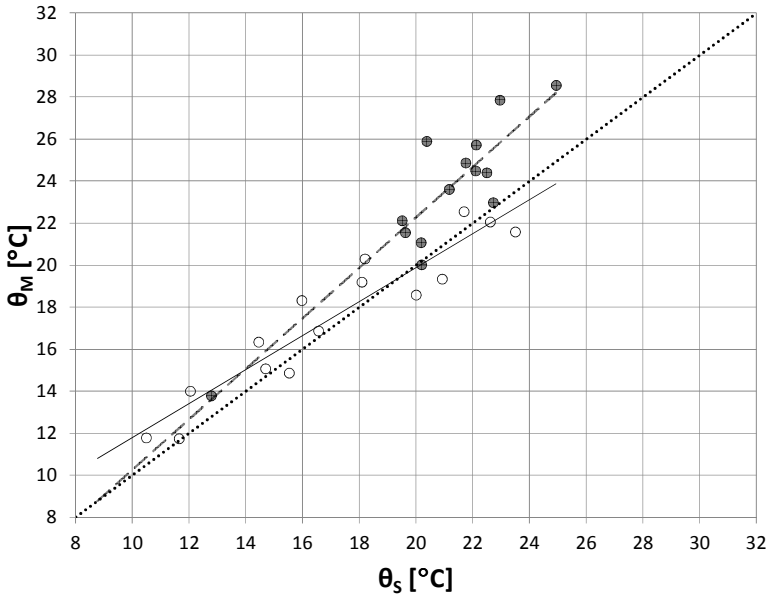

Figure 52: Mobile versus stationary air temperature measurements, mobile spot location B1 (white dots + solid regression coefficient line: morning measurements; dark dots + dashed regression coefficient line: afternoon measurements; dotted line: theoretical line of perfect agreement)

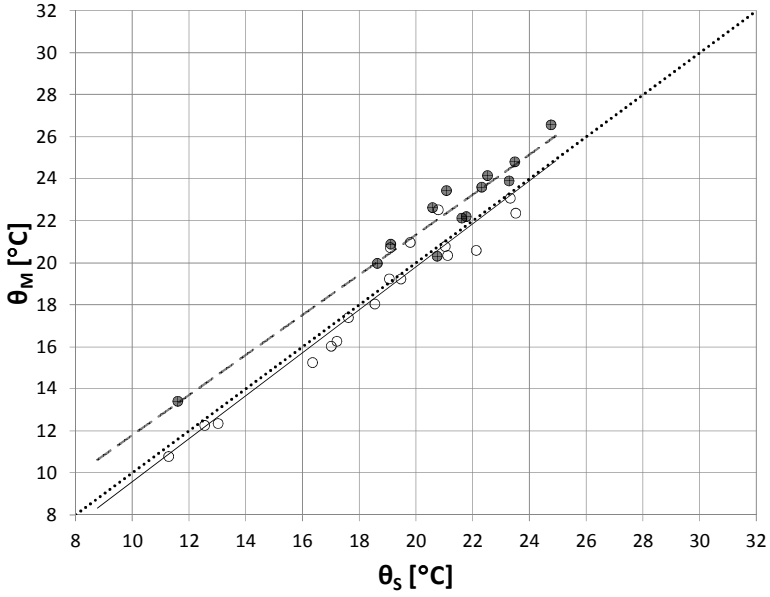

Figure 53: Mobile versus stationary air temperature measurements, mobile spot location B2 (white dots + solid regression coefficient line: morning measurements; dark dots + dashed regression coefficient line: afternoon measurements; dotted line: theoretical line of perfect agreement)

4.4.2.3 WEATHER STATION MEASUREMENTS – AREA C

The mobile versus stationary weather station measurements for area C is graphed for analysis (Figure 54 and Figure 55). The mobile data points from these two spot locations (C1 and C2) are compared with the simultaneously monitored stationary weather station measurement in spot location C0 (diagonal dotted line in the graphs).

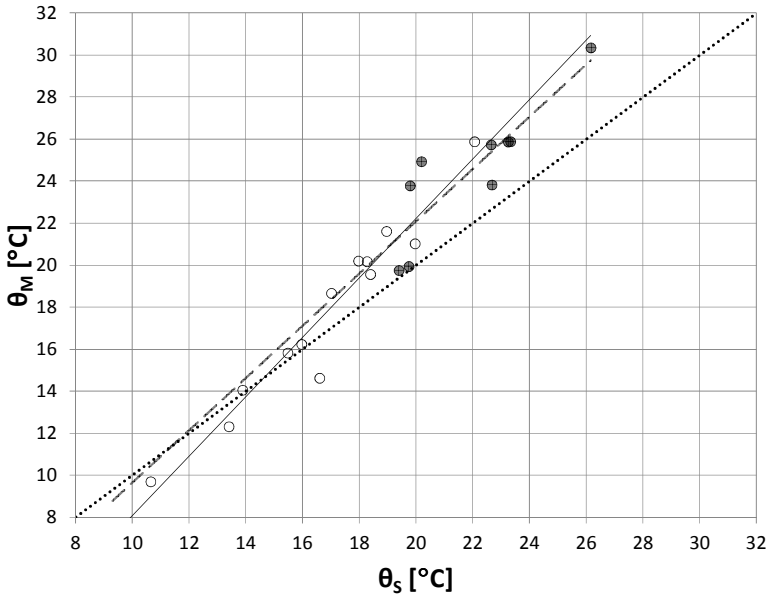

Figure 54: Mobile versus stationary air temperature measurements, mobile spot location C1 (white dots + solid regression coefficient line: morning measurements; dark dots + dashed regression coefficient line: afternoon measurements; dotted line: theoretical line of perfect agreement)

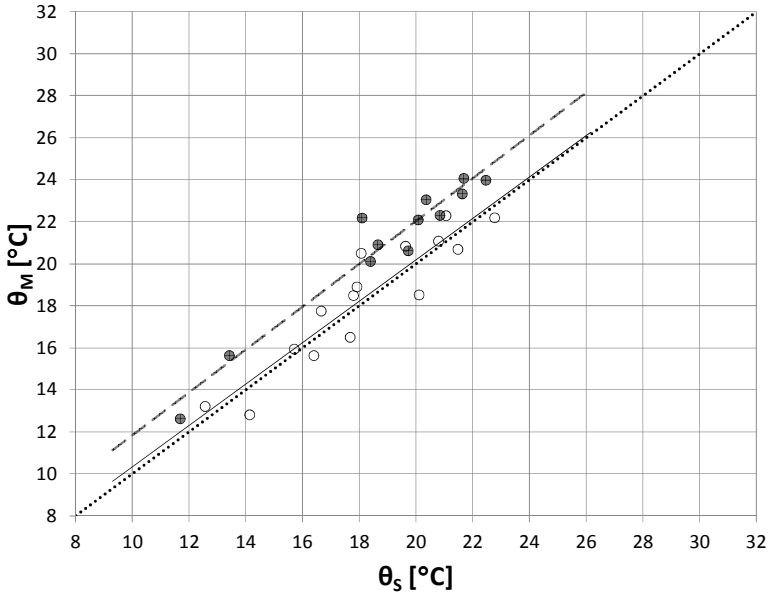

Figure 55: Mobile versus stationary air temperature measurements, mobile spot location C2 (white dots + solid regression coefficient line: morning measurements; dark dots + dashed regression coefficient line: afternoon measurements; dotted line: theoretical line of perfect agreement)

4.4.2.4 WEATHER STATION MEASUREMENTS – AREA D

The mobile versus stationary weather station measurements for area D is graphed for analysis (Figure 56 and Figure 57). The mobile data points from these two spot locations (D1 and D2) are compared with the simultaneously monitored stationary weather station measurement in spot location D0 (diagonal dotted line in the graphs).

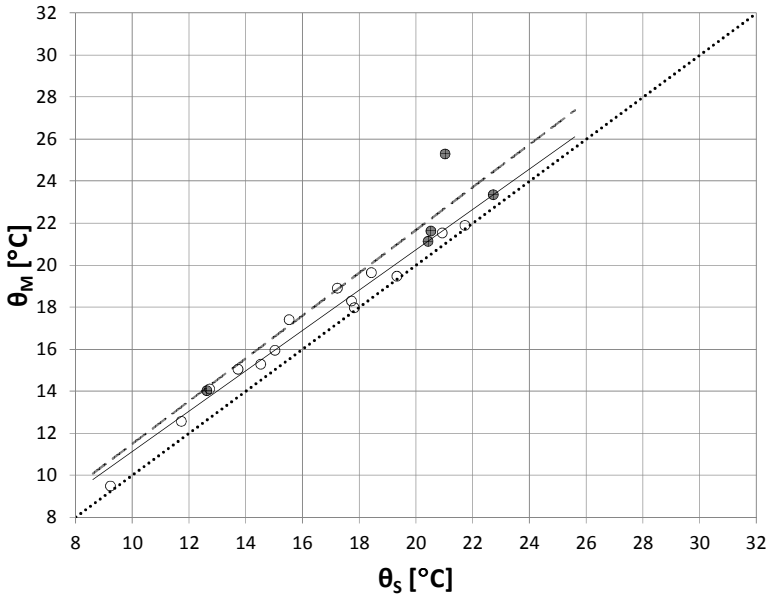

Figure 56: Mobile versus stationary air temperature measurements, mobile spot location D1 (white dots + solid regression coefficient line: morning measurements; dark dots + dashed regression coefficient line: afternoon measurements; dotted line: theoretical line of perfect agreement)

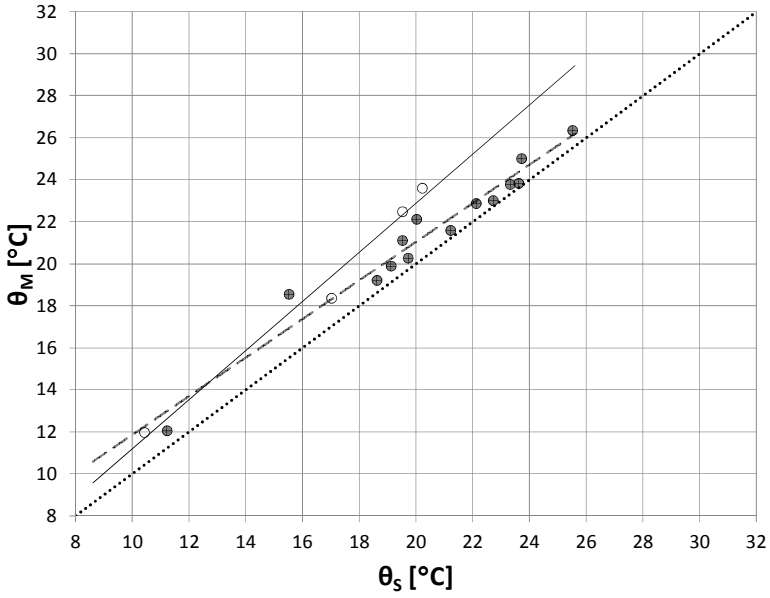

Figure 57: Mobile versus stationary air temperature measurements, mobile spot location D2 (white dots + solid regression coefficient line: morning measurements; dark dots + dashed regression coefficient line: afternoon measurements; dotted line: theoretical line of perfect agreement)

4.4.2.5 WEATHER STATION MEASUREMENTS – AREA E

The mobile versus stationary weather station measurements for area E is graphed for analysis (Figure 58 and Figure 59). The mobile data points from these two spot locations (E1 and E2) are compared with the simultaneously monitored stationary weather station measurement in spot location E0 (diagonal dotted line in the graphs).

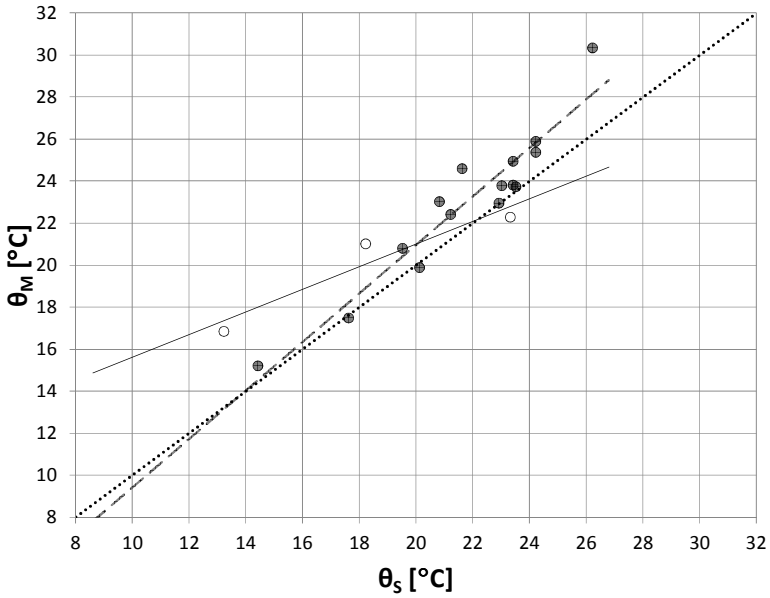

Figure 58: Mobile versus stationary air temperature measurements, mobile spot location E1 (white dots + solid regression coefficient line: morning measurements; dark dots + dashed regression coefficient line: afternoon measurements; dotted line: theoretical line of perfect agreement)

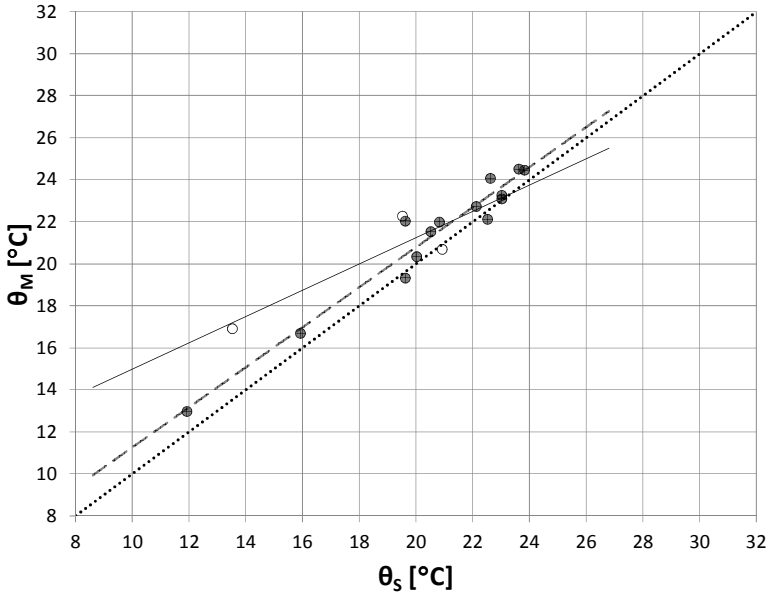

Figure 59: Mobile versus stationary air temperature measurements, mobile spot location E2 (white dots + solid regression coefficient line: morning measurements; dark dots + dashed regression coefficient line: afternoon measurements; dotted line: theoretical line of perfect agreement)

4.4.3 DISCUSSION OF MICROCLIMATE ANALYSIS

Analyses of the weather station air temperature measurements were performed. Valid data points from mobile weather stations in each area were compared with their simultaneously monitored stationary weather station.

The results corroborate the finding of the overall mobile weather station measurements versus stationary weather station analysis (see Figure 49). In addition, the graphs display mobile air temperature measurements are systematically higher than their respective stationary stations.

In a physically similar site condition, such as conditions found in area A, the graphs displays a strong correlation of mobile measurements to their reference stationary weather station in both spot locations (see Figure 50 and Figure 51). The mobile locations in this area and the reference stationary weather station are highly representative of the nearby urban circumstance and thus the difference between stationary and mobile weather station data are rather small.

Areas B through E, on the other hand, did not display any significant correlation in mobile air temperature measurements, suggesting that these differences are arguably due to the specific urban conditions (morphology, property of the surfaces in the surroundings, fraction of visible sky, etc.). Mobile air temperature measurements in the afternoon hours were systematically higher than their respective stationary stations.

It can be concluded that in an area with similar urban circumstances, the difference in regression coefficient values of mobile and stationary air measurements is rather small, such as in case of area A. Although areas B through E did not display any consistent trend, air temperature measurements in the afternoon hours were systematically higher than stationary weather station.

4.5 UHI INTENSITY ANALYSIS OF WEATHER STATIONS MEASUREMENTS

The finalized dataset used for the air temperature correlation analysis also serves as a basis for the following UHI intensity analysis of the weather station air temperature measurements. This dataset, consisting of one stationary and two mobile measurements of each of the five study areas was averaged to form two sets of values for each area, five in the morning and five in the afternoon; producing a total of 10 data points (Table 10).

This part of the research analyzes the UHI intensity in two parts. First part of this analysis discusses the UHI intensity of mobile versus stationary weather station measurements. The second part discusses the relationship of UHI intensity versus selected U2O variables. Overall values of the U2O variables for each area are presented in this portion of the research (Table 12). Seibersdorf weather monitoring station serves as a rural basis for calculating the UHI intensity.

Area A is isolated in the mobile versus stationary UHI intensity analysis for several reasons (see Figure 25 and Figure 26). The monitoring mobile units in that area were differently equipped from the other four areas; namely better shielding which resulted in no statistical outliers. And, in area A, monitoring at the two spot locations was done simultaneously, effectively doubling the monitored data points and there was no need to switch locations hourly.

In this section, there are two questions that this research addresses: 1) how does the morphological difference of the study areas affect the variance of the UHI intensity correlation? 2) what is the level of agreement of the correlation coefficient that can be concluded from this analysis?

4.5.1 UHI INTENSITY CORRELATION – MOBILE VERSUS STATIONARY WEATHER STATION MEASUREMENTS

The graph below (Figure 60) compares the UHI intensity for the mobile weather stations (UHI_M) with the simultaneously monitored data from the reference stationary weather stations (UHI_S); white triangles represent mobile measurements.

Unlike the air temperature correlation analysis (Figure 48), the graph does not display any pattern of agreement of the UHI intensity between the mobile and stationary weather station measurements. Average value of UHI intensity for each study area (Table 10) displays a systematically higher UHI intensity value during the afternoon hours compared to morning hours.

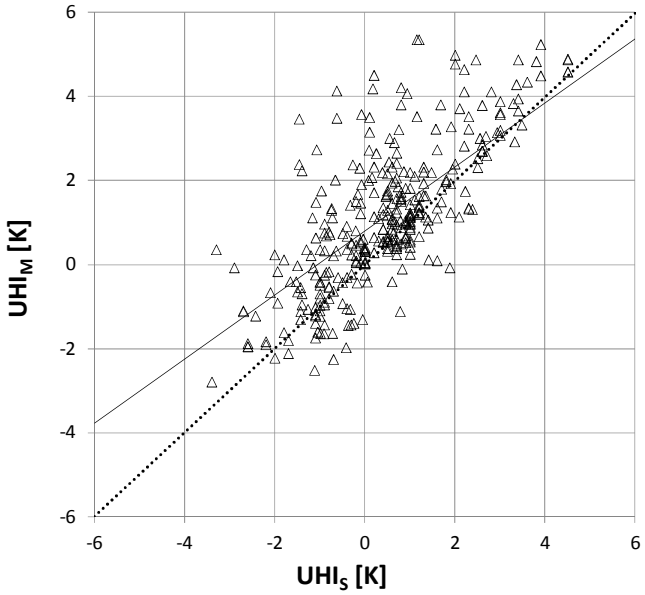

Figure 60: Mobile versus stationary UHI intensity (white triangles; continuous line represent regression coefficient line for mobile measurements in all areas versus reference stationary weather stations (dotted line)

Table 10: Average value of UHI intensity for each study area

	Study area	UH intensity morning [K]	UHI intensity afternoon [K]
A	Innere Stadt	0.10	1.45
B	Gaudenzdorf	0.12	1.74
C	AKH	0.51	1.61
D	Hohe Warte	0.96	1.54
E	Donaufeld	0.21	1.88

4.5.1.1 WEATHER STATION UHI INTENSITY – AREA A

The UHI intensity for area A, comparing mobile versus stationary weather stations, is graphed for analysis (Figure 61 and Figure 62). The morphological surroundings of all three weather stations (one stationary and two mobile) in this area are similar. The graphs display strong correlation, especially during the afternoon hours for stationary (A0) and mobile weather station (A1 and A2) spot locations.

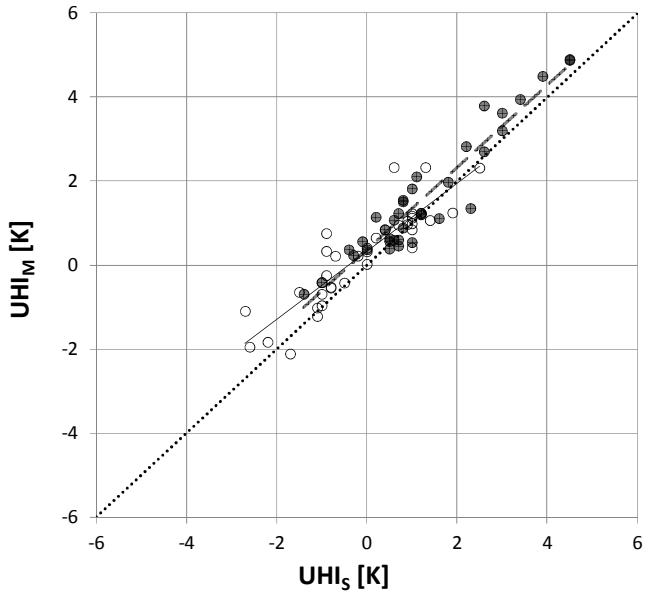

Figure 61: Mobile versus stationary UHI intensity, mobile spot location A1 (white dots + solid regression coefficient line: morning measurements; dark dots + dashed regression coefficient line: afternoon measurements)

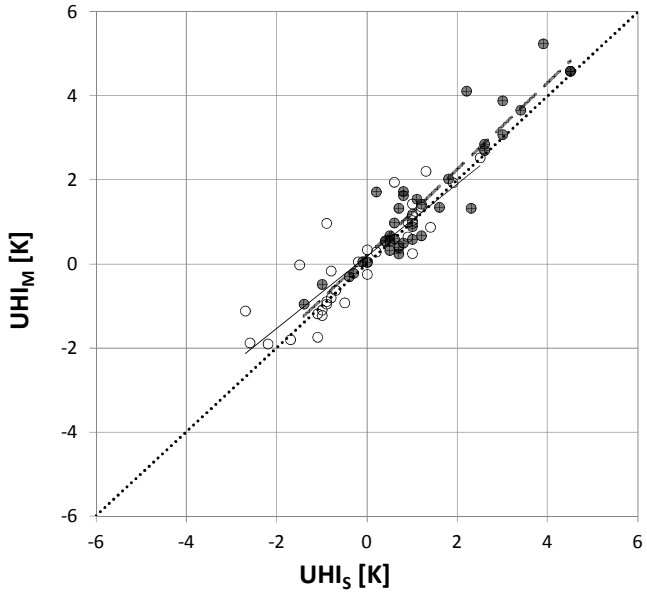

Figure 62: Mobile versus stationary UHI intensity, mobile spot location A2 (white dots + solid regression coefficient line: morning measurements; dark dots + dashed regression coefficient line: afternoon measurements)

4.5.1.2 WEATHER STATION UHI INTENSITY – AREAS B THROUGH E

The UHI intensity for areas B through E, comparing mobile versus stationary weather station, is graphed for analysis (Figure 63 and Figure 64). The morphological surroundings of all three weather stations (stationary and mobile) in these areas were dissimilar. The graphs display very weak correlation in all spot locations.

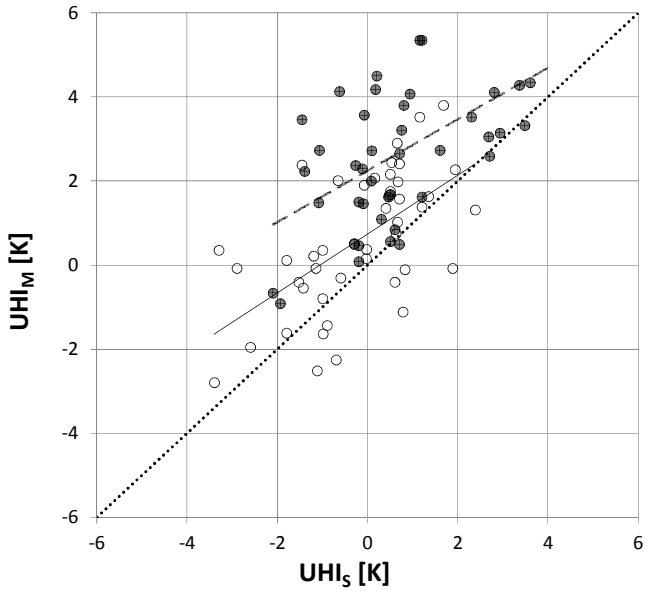

Figure 63: Mobile versus stationary UHI intensity, mobile spot locations 1 (white dots + solid regression coefficient line: morning measurements; dark dots + dashed regression coefficient line: afternoon measurements)

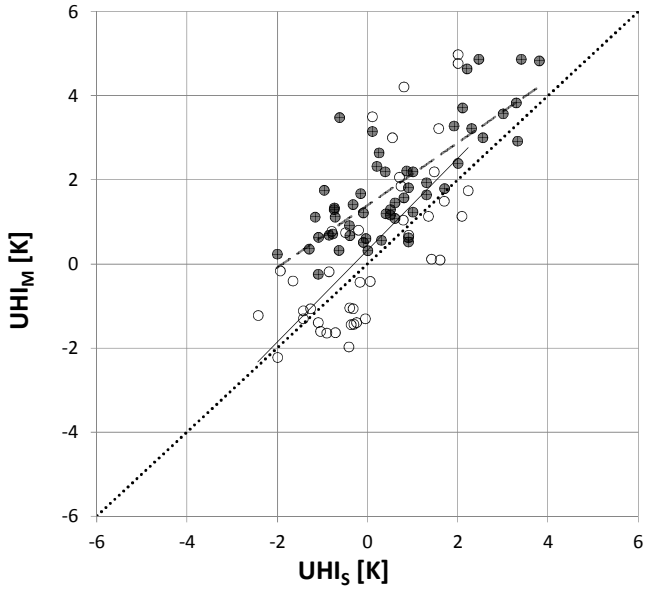

Figure 64: Mobile versus stationary UHI intensity, mobile spot locations 2 (white dots + solid regression coefficient line: morning measurements; dark dots + dashed regression coefficient line: afternoon measurements)

4.5.2 UHI INTENSITY CORRELATION –WEATHER STATION MEASUREMENTS VERSUS U2O VARIABLES

Specific urban conditions in the measured study areas can have a profound impact on affecting the variability on the microclimate. Therefore, four selected contributing factors for the five study areas: urban geometry, urban sealing, urban density, and anthropogenic heat generation as set forth by U2O framework (Table 11), are analyzed versus the UHI intensity.

Table 11: Four selected influencing factors: sky view factor, impervious surface fraction, mean building compactness, and anthropogenic heat output

Influencing Factors	Symbol	Definition
Sky View Factor	ψ_{sky}	Mean value of the fraction of sky hemisphere visible from ground level
Impervious surface fraction	A_i	Ratio of unbuilt impervious plan area (paved, sealed) to total ground area
Mean building compactness	$l_c = V_b / A_b$	Ratio of built volume (above terrain) to total building plan area
	V_b : built volume [m^3]	total built volume, above ground
	A_b : built area [m^2]	total building footprint
Anthropogenic heat output	Q_F	Mean annual heat flux density from fuel combustion and human activity (traffic, industry, heating and cooling of buildings, etc.)

The basis of the U2O framework is to ascertain the specific characteristic features of an area in the context of their geometry, massing, or other physical aspects in context of contributing factors of UHI. The calculated values for U2O for the five mobile locations are provided, in whole, by Vuckovic (2014) as part of her dissertation research (Table 12).

Table 12: Selected U2O variables. Source: (Vuckovic 2014)

Study area	Overall sky view factor	Overall area impervious surface fraction	Overall area mean building compactness	Overall area anthropogenic heat output
A	0.47	45%	23.35m	350 $W \cdot m^{-2}$
B	0.51	46%	13.56m	430 $W \cdot m^{-2}$
C	0.49	44%	13.50m	419 $W \cdot m^{-2}$
D	0.59	34%	8.00m	177 $W \cdot m^{-2}$
E	0.75	31%	6.15m	89 $W \cdot m^{-2}$

4.5.2.1 WEATHER STATION UHI INTENSITY VERSUS SKY VIEW FACTOR

Average value of UHI intensity for the five study areas (see Table 10) versus sky view factor is graphed below (Figure 65).

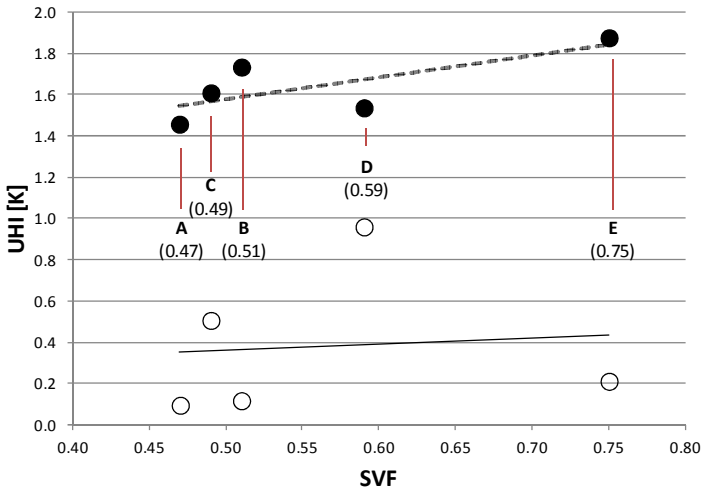

Figure 65: UHI intensity versus sky view factor for areas A-E (white dots + solid regression coefficient line: morning measurements; dark dots + dashed regression coefficient line: afternoon measurements)

4.5.2.2 WEATHER STATION UHI INTENSITY VERSUS IMPERVIOUS SURFACE FRACTION

Average value of UHI intensity for the five study areas (see Table 10) versus impervious surface fraction is graphed below (Figure 66).

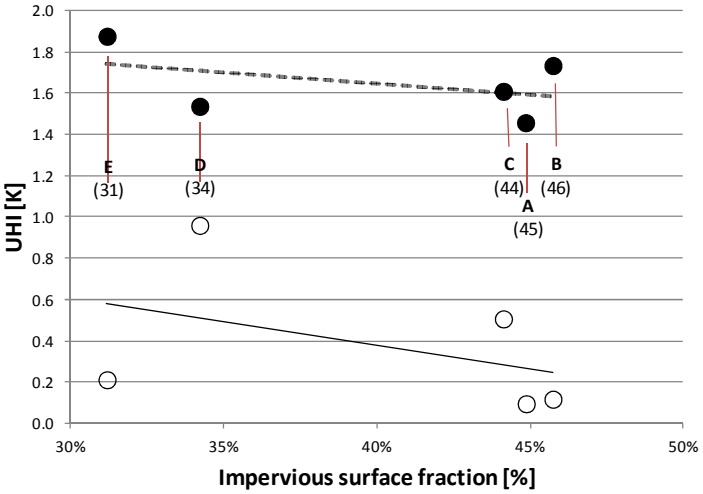

Figure 66: UHI intensity versus impervious surface fraction for areas A-E (white dots + solid regression coefficient line: morning measurements; dark dots + dashed regression coefficient line: afternoon measurements)

4.5.2.3 WEATHER STATION UHI INTENSITY VERSUS MEAN BUILDING COMPACTNESS

Average value of UHI intensity for the five study areas (see Table 10) versus mean building compactness is graphed below (Figure 67).

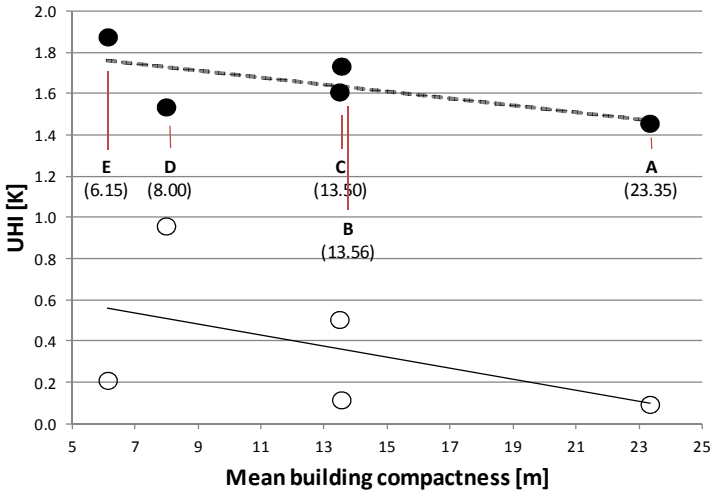

Figure 67: UHI intensity versus mean building compactness for areas A-E (white dots + solid regression coefficient line: morning measurements; dark dots + dashed regression coefficient line: afternoon measurements)

4.5.2.4 WEATHER STATION UHI INTENSITY VERSUS ANTHROPOGENIC HEAT OUTPUT

Average value of UHI intensity for the five study areas (see Table 10) versus anthropogenic heat output is graphed below (Figure 68).

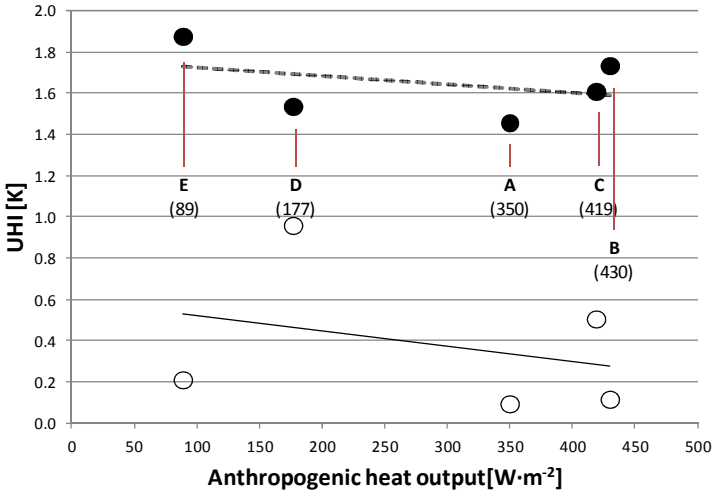

Figure 68: UHI intensity versus anthropogenic heat output for areas A-E (white dots + solid regression coefficient line: morning measurements; dark dots + dashed regression coefficient line: afternoon measurements)

4.5.3 DISCUSSION OF UHI INTENSITY ANALYSIS

Analyses of UHI intensity versus four selected contributing factors were performed. Valid data points from mobile weather stations in each area were compared with their simultaneously monitored stationary weather station.

Area A, where the morphological surroundings of all three weather stations (stationary and mobile) were similar, displayed a relatively strong correlation of UHI intensity in both spot locations (see Figure 61 and Figure 62). UHI intensity was systematically higher in the afternoon than in the morning hours in the study areas.

As previously discussed in section 4.3.4, a total of 59 statistical outliers were removed by employing method B – the modified Thompson's tau technique. Most of the removed data points were located in areas B, D and E (see Figure 47). Therefore, these areas lacked sufficient valid data points, and did not display any significant correlation in mobile air temperature measurements (see Figure 63 and Figure 64).

Studying the graphs may suggest there is a trend forming between the contributing factors and regression values of the mobile air temperature measurements in the study areas. However, this finding is speculative and deserves further investigation in order to reduce a "chance" correlation; a simple correlation is not sufficient measure of agreement.

5. CONCLUSION

5.1 CONTRIBUTIONS

This research was carried out for five city locations in Vienna, Austria, to investigate how microclimate variation can occur due to diverse site conditions. One stationary and two mobile weather stations in each study area were monitored for two one-week periods: one week in spring and one week in summer. Mobile air temperature measurements were quality-checked by removing outliers. Microclimate and UHI intensity analyses for each of the locations were performed. In addition, four selected factors were compared in order to explore their possible role in influencing the UHI intensity.

The main objective of the study was to ascertain if there are differences between data obtained from standard (stationary) weather stations and those located in an urban canyon or in an open-field. The research found, beside the urban geometry, other factors such as urban sealing, density, and anthropogenic heat output can have an equal or greater role in influencing the microclimate in an urban canyon. However, the degree of this role is not yet clear based on the data monitored in the study areas.

The findings of this research corroborate past and on-going research that heat islands in urban areas tend to display a typical pattern, that the intensity can be quite different at each location, even in close proximity of each other. Much of this may be due to the unique environmental conditions that make up an urban canyon. Even then, the mobile locations can differ quite significantly within the five study areas. However, if a stationary weather station is located in a position highly representative of the nearby urban circumstance (in this case, area A), then the differences between stationary and mobile weather station data are rather small.

Despite best efforts to quality-check the monitored mobile dataset for outliers, it is difficult to establish a direct cause-and-effect between UHI intensity and the selected contributing factors (see Figure 65 through Figure 68). Possible reasons could be that there is a third variable that is not yet known related to both of the variables being investigated, which may be responsible for the apparent correlation. Also, a nonlinear relationship may exist between the two variables that would be inadequately described or possibly even undetected by the correlation coefficient.

Even though a clear cause-and-effect cannot be established from the findings of this research, it is worthwhile to present the quality-checking techniques for the dataset and provide the methodology to assess the dataset in order to further the understanding of this complex phenomenon.

The methodology presented in this research gives another systematic approach to understanding the complex UHI phenomenon. Furthermore, it introduced a technique for quality-checking questionable dataset. However, this does not make up for the lack of data points. Two mobile monitoring units in area A, which had no outliers removed by method B (see section 4.3.2), had the strongest relationship to their respective stationary weather station. Whereas areas B through E started with less than half the number of data point as area A and in some cases lost another half due to the quality-check process. The remaining data points were statistically relevant, but the results may have been skewed due to loss of fidelity in the dataset.

The research concludes that when microclimatic data from stationary weather stations are used for decision making processes (e.g., building design and retrofit applications), potential differences between such data and actual conditions within the urban fabric (e.g., at the specific location of planned interventions) must be taken into consideration.

5.2 FUTURE RESEARCH

Future research can investigate utility of specific transfer functions that would allow for the derivation of site-specific microclimatic information from data provided by near-by stationary weather stations.

REFERENCES

BIBLIOGRAPHY

Akbari, H., Pomerantz, M., Taha, H. 2001. Cool surfaces and shade trees to reduce energy use and improve air quality in urban areas. Solar energy, Volume 70, Issue 3 :295–310.

Alexandri E., Jones P. 2004. The Thermal Effects of Green Roofs and Green Facades on an Urban Canyon (pp. 19–22). Presented at the The 21th Conference on Passive and Low Energy Architecture, Eindhoven, The Netherlands.

Alexandri E., Jones P. 2006. Sustainable Urban Futures in Southern Europe-What about the Heat Island Effect? In ERSA conference papers (pp. 1–26). Presented at the Environment, Natural Resources and Sustainability.

Alexandri E., Jones P. 2008. Temperature decreases in an urban canyon due to green walls and green roofs in diverse climates. Building and Environment, Volume 43, Issue 4 :480–493.

Ali-Toudert F. 2005. Dependence of Outdoor Thermal Comfort on Street Design in Hot and Dry Climate (Dissertation). Universität Freiburg, Freiburg, Germany. Retrieved from http://www.meteo.uni-freiburg.de/forschung/publikationen/berichte/report15.pdf

Ali-Toudert, F., Mayer, H. 2006a. Effects of street design on outdoor thermal comfort :45–55.

Ali-Toudert, F., Mayer, H. 2006b. Numerical study on the effects of aspect ratio and orientation of an urban street canyon on outdoor thermal comfort in hot and dry climate. Building and Environment, Volume 41, Issue 2 :94–108.

Amtmann M. 2011. Reference buildings - The Austrian building typology (pp. 1–57).

Beatley T. 2000. Green urbanism: learning from European cities. Washington, DC: Island Press.

Berdahl P., Bretz S. E. 1997. Preliminary survey of the solar reflectance of cool roofing materials. Energy and Buildings, Volume 25, Issue 2 :149–158.

Böhm R. 1998. Urban Bias in Temperature Time Series – a Case Study for the City of Vienna, Austria. Climatic Change, Volume 38, :113–128.

Bouyer J., Musy M., Huang Y., Athamena K. 2009. Mitigating urban heat island effect by urban design: forms and materials. In Proceedings of the 5th urban research symposium, cities and climate change: responding to an urgent agenda, Marseille (pp. 28–30).

Buccolieri R., Gromke C., Di Sabatino S., Ruck B. 2009. Aerodynamic effects of trees on pollutant concentration in street canyons. Science of The Total Environment, Volume 407, Issue 19 :5247–5256.

Castleton H. F., Stovin V., Beck S. B. M., Davison J. B. 2010. Green roofs; building energy savings and the potential for retrofit. Energy and Buildings, Volume 42, Issue 10 :1582–1591.

Christopherson R. 2012. Elemental Geosystems (7th Edition.). Prentice Hall.

Cimbala J. M. 2011, September 12. Outliers. Retrieved from http://www.mne.psu.edu/me345/Lectures/Outliers.pdf

Deb C., Ramachandraiah A. 2011. A simple technique to classify urban locations with respect to human thermal comfort: Proposing the HXG scale. Building and Environment, Volume 46, Issue 6 :1321–1328.

Doya M., Bozonnet E., Allard F. 2012. Experimental measurement of cool facades' performance in a dense urban environment. Energy and Buildings, Volume 55, :42–50.

Eliasson I. 1996. Urban nocturnal temperatures, street geometry and land use. Atmospheric Environment, Volume 30, Issue 3 :379–392.

Fahmy M., Hathway A., Pattacini L., Elwan A. 2011. Environmental thermal impact assessment of regenerated urban form: A case study in Sheffield. In World Renewable Energy Congress 2011.

Für eine offene Stadt - Open Government Wien. (accessed 2013). Für eine offene Stadt - Open Government Wien. Retrieved from https://open.wien.at/

Gago E. J., Roldan J., Pacheco-Torres R., Ordóñez J. 2013. The city and urban heat islands: A review of strategies to mitigate adverse effects. Renewable and Sustainable Energy Reviews, Volume 25, :749–758.

Gál T., Lindberg F., Unger J. 2008. Computing continuous sky view factors using 3D urban raster and vector databases: comparison and application to urban climate. Theoretical and Applied Climatology, Volume 95, Issue 1-2 :111–123.

Gartland L. 2008. Heat Islands - Understanding and Mitigating Heat in Urban Areas. Earthscan.

Giannopoulou K., Santamouris M., Livada I., Georgakis C., Caouris Y. 2010. The Impact of Canyon Geometry on Intra Urban and Urban: Suburban Night Temperature Differences Under Warm Weather Conditions. Pure and Applied Geophysics, Volume 167, Issue 11 :1433–1449.

Hammerberg K. 2014, January 22. Accounting for the Role of Trees in Urban Energy Balance Modeling Using GIS Techniques. (Master of Science). Vienna University of Technology, Vienna, Austria.

Hebbert M., Jankovic V., Webb B. 2011. City weathers: meteorology and urban design 1950-2010. University of Manchester: Manchester Architecture Research Centre.

Hirschler P., Svanda N. 2009. Moving in Vienna – intelligence "on the move." In 45th ISOCARP Congress 2009.

Holmer B. 1992. A simple operative method for determinating of sky view factors in complex urban canyons from fisheye photographs. Meteorologische Zeitschrift, :236–239.

Human footprint: Wie wir die Welt verändern. 2011, September 27. News.AT. Retrieved from http://www.news.at/a/human-footprint-wie-welt-307970/slide-11

Johnson G. T., Oke T. R., Lyons T. J., Steyn D. G., Watson I. D., Voogt J. A. 1991. Simulation of surface urban heat islands under "ideal"conditions at night Part 1: theory and tests against field data. Boundary-Layer Meteorology, Volume 56, Issue 3 :275–294.

Johnson G. T., Watson I. D. 1984. The Determination of View-Factors in Urban Canyons. Journal of Climate and Applied Meteorology, Volume 23, Issue 2 :329–335.

Kiesel K., Vuckovic M., Orehounig K., Mahdavi A. 2012. Analysis of micro climatic variations and the urban heat island phenomenon in the city of Vienna. Presented at the EURA 2012 conference, Vienna, Austria.

Kosareo L., Ries R. 2007. Comparative environmental life cycle assessment of green roofs. Building and Environment, Volume 42, Issue 7 :2606–2613.

Lafrance M. 2009. Assessment of International Urban Heat Island Research: Review and Critical Analysis of International UHI Studies. Navigant Consulting, Inc.

Lechleitner J. 2005. Wetterstation der TU.ppt.

Lindberg F., Eliasson I., Holmer B. 2003. Urban geometry and temperature variations. In Proc. 5th Int Conf Urban Climate (Vol. 1, pp. 205–208).

Mahdavi A., Kiesel K., Vuckovic M. 2013. A framework for the evaluation of urban heat island mitigation measures. Presented at the SB13 Munich Conference, Munich, Germany.

Maleki A., Orehounig K., Mahdavi A. 2012. Monitoring and modeling of the urban micro-climate. In First International Conference on Architecture and Urban Design (pp. 1019–1028). Presented at the 1-ICAUD, Tirana, Albania.

Moore D. S., McCabe G. P., Craig B. A. 2009. Introduction to the practice of statistics extended version. New York: W.H. Freeman.

Nunez M., Oke T. R. 1977. The energy balance of an Urban Canyon. Journal of Applied Meteorology, Volume 16, :11–19.

Offerle B., Grimmond C. S. B., Fortuniak K. 2005. Heat storage and anthropogenic heat flux in relation to the energy balance of a central European city centre. International Journal of Climatology, Volume 25, Issue 10 :1405–1419.

Oke T. R. 1973. City size and the urban heat island. Atmospheric Environment (1967), Volume 7, Issue 8 :769–779.

Oke T. R. 1982. The energetic basis of the urban heat island. Quarterly Journal of the Royal Meteorological Society, Volume 108, Issue 455 :1–24.

Oke T. R. 1992. Boundary layer climates. London; New York: Routledge.

Olivieri F., Vidal P., Guerra R., Chanampa M., Garcia J., Bedoya C. 2012. Green Facades for Urban Comfort Improvement. In PLEA2012 - 28th Conference (p. 6). Presented at the Opportunities, Limits & Needs Towards an environmentally responsible architecture, Lima, Peru.

Orehounig K., Kiesel K., Mahdavi A. 2012. Derivation of locally adjusted high-resolution weather information for building performance simulation. In Fourth German-Austrian IBPSA Conference (pp. 104–109). Presented at the BauSIM 2012, Berlin, Germany.

Park M., Hagishima A., Tanimoto J., Narita K. 2012. Effect of urban vegetation on outdoor thermal environment: Field measurement at a scale model site. Building and Environment, Volume 56, :38–46.

Pigeon G., Legain D., Durand P., Masson V. 2007. Anthropogenic heat release in an old European agglomeration (Toulouse, France). International Journal of Climatology, Volume 27, Issue 14 :1969–1981.

Population forecast for Vienna 2011-2075. 2012, September 14. Statistik Austria. Retrieved from https://www.statistik.at/web_en/statistics/population/demographic_forecasts/population_forecasts/index.html

Population growth in Vienna. 2009. Statistik Austria. Retrieved from https://www.statistik.at/web_en/statistics/population/demographic_forecasts/population_forecasts/index.html

Quah A. K. L., Roth M. 2012. Diurnal and weekly variation of anthropogenic heat emissions in a tropical city, Singapore. Atmospheric Environment, Volume 46, :92–103.

Ratti C., Bakerb N., Steemers K. 2004. Urban texture and radiation exchange.

Ratti C., Richens P. 1999. Urban texture analysis with image processing techniques. In Computers in Building (pp. 49–64). Springer.

Reducing Urban Heat Islands: Compendium of Strategies. (accessed 2013). U.S. Environmental Protection Agency.

Robitu M., Musy M., Inard C., Groleau D. 2006. Modeling the influence of vegetation and water pond on urban microclimate. Solar Energy, Volume 80, Issue 4 :435–447.

Roof mounted BPI weather station. 2014. Vienna University of Technology - Department of Building Physics and Building Ecology.

Sailor D. J. 2007. The Urban Heat Island (UHI) - Causes, Impacts, and Mitigation Strategies. Presented at the State Clean Energy-Environmental Technical Forum.

Sailor D. J., Lu L. 2004. A top–down methodology for developing diurnal and seasonal anthropogenic heating profiles for urban areas. Atmospheric Environment, Volume 38, Issue 17 :2737–2748.

Saneinejad S., Moonen P., Defraeye T., Derome D., Carmeliet J. 2012. Coupled CFD, radiation and porous media transport model for evaluating evaporative cooling in an urban environment. Journal of Wind Engineering and Industrial Aerodynamics, Volume 104–106, :455–463.

Sonne J. 2006. Evaluating green roof energy performance. ASHRAE JOURNAL, Volume 48, Issue 2 :59.

Spangenberg J., Shinzato P., Johansson E., Duarte D. 2008. Simulation of the influence of vegetation on microclimate and thermal comfort in the city of São Paulo. Revista SBAU, Piracicaba, Volume 3, Issue 2 :1–19.

Stationsbeschreibung & Standortsklimatologie. 2010. Zentralanstalt für Meteorologie und Geodynamik. Retrieved from http://wms1.zamg.ac.at/beauvort/pdfs/Wien_Innere_Stadt.pdf

Stewart I. D., Oke T. R. 2012. Local Climate Zones for Urban Temperature Studies. Bulletin of the American Meteorological Society, Volume 93, Issue 12 :1879–1900.

Strauss F., Formayer H., Asamer V., Schmid E. 2010. Climate change data for Austria and the period 2008-2040 with one day and km2 resolution.

Takebayashi H., Moriyama M. 2009. Study on the urban heat island mitigation effect achieved by converting to grass-covered parking. Solar Energy, Volume 83, Issue 8 :1211–1223.

Tennis P. D., Leming M. L., Akers D. J. 2004. Pervious concrete pavements. Skokie, Ill.: Portland Cement Association.

Thompson W. R. 1935. On a Criterion for the Rejection of Observations and the Distribution of the Ratio of Deviation to Sample Standard Deviation. The Annals of Mathematical Statistics, Volume 6, Issue 4 :214–219.

Thundiyil K. A. 1998. Rising Temperatures and Expanding Megacities: Improving Air Quality in Mexico City through Urban Heat Island Mitigation. Massachusetts Institute of Technology.

Vienna City Administration - Municipal Department 23. 2012. Vienna in Figures 2012. Retrieved from http://www.wien.gv.at/statistik/pdf/viennainfigures.pdf

Vuckovic M. 2014. Personal correspondance regarding microclimate variability in Vienna, Austria.

Zhang J., Heng C. K., Malone-Lee L. C., Hii D. J. C., Janssen P., Leung K. S., Tan B. K. 2012. Evaluating environmental implications of density: A comparative case study on the relationship between density, urban block typology and sky exposure. Automation in Construction, Volume 22, :90–101.

LIST OF TABLES

LIST OF FIGURES

LIST OF EQUATIONS

ABBREVIATIONS

Symbol	Name	Unit
a.g.l.	above ground level	m
A	slope angle	°
a_b	albedo (reflectivity) of a person's body surface	
a_{cl}	albedo of clothing	
a_g	albedo of the ground surface	
a_o	mean albedo of ground-based, solid objects projecting into the sky hemisphere, especially building surfaces	
a_{veg}	albedo of vegetation (tree) surface	
B	the Bowen ratio	
c	specific heat capacity	$Jkg^{-1}K^{-1}$
ε	thermal emittance, emissivity	
G_0	global solar radiation	Wm^{-2}
h	a height above sea level	m
H	building height	m
k, λ	thermal conductivity	$Wm^{-1}K^{-1}$
$K\downarrow$	total incoming solar radiation from the sky hemisphere incident on the (human body) surface	Wm^{-2}
$K\uparrow$	total solar radiation from the ground hemisphere incident on the (human body) surface	Wm^{-2}
K_b	incoming direct beam solar radiation on a horizontal surface	Wm^{-2}
T_{mrt}	mean radiant temperature	
T_s	surface temperature	°C
ψ_s, SVF	sky view factor	
Q*	net wave radiation	
Q_F	anthropogenic heat flux	
Q_H	convective sensible heat flux	
Q_E	latent heat flux	
ΔQ_S	net storage heat flux	
ΔQ_A	advection	
EPA	U.S. Environmental Protection Agency	
IS	Innere Stadt (Vienna city center)	
HW	Höhewarte	
AKH	Allgemeines Krankenhaus der Stadt Wien (Vienna General Hospital)	
DF	Donbaufeld	
GD	Gaudenzdorf	
BPI	Department of Building Physics and Building Ecology	
SW	Stadt Wien (City of Vienna)	
UHI	Urban Heat Island	
U2O	Urban Unit of Observation framework	
ZAMG	Zentralanstalt für Meteorologie und Geodynamik (Central Institute for Meteorology and Geodynamics)	
u.o.n.	unless otherwise noted	

APPENDIX A: BUILDING TYPOLOGY

Table 13: Building typology. Source: (Amtmann 2011)

				U-value						Typ. heating load (kWh/m-				
built year	from	to		roof	ceiling	wall	windov	slab/basement		lower	upper	actual	renov.	renov. 2
I	-	1918		1.70	1.10	1.40	2.20	1.20		180	300			
II	1919	1944		1.70	0.80	1.40	2.30	1.20		200	370			
III	1945	1959		1.70	0.80	1.30	2.30	1.20		160	380			
IV	1960	1979		0.80	0.70	1.10	2.70	0.80		145	280			
V	1980	1989		0.50	0.40	0.60	2.50	0.50		100	190			
VI	1990	1999		0.30	0.30	0.40	1.80	0.50		80	130			
VII	2000	2010		0.20	0.20	0.35	1.40	0.40		10	100			
actual examples														
I	-	1918			0.51	1.10	3.10	0.95				133		
						0.35							76	
					0.15	0.20	1.00							30
II	1920	1944			0.68	1.16	2.30	0.78				130		
						0.35							78	
						0.10	1.00							30
III	1945	1959			0.90	0.90	2.30	1.07				136		
					0.20	0.32	1.40						51	
					0.20	0.15	1.00	0.30						30
IV	1960	1979			1.83	0.36	1.76	1.83				121		
					0.40			0.40					83	
					0.15	0.20	1.00	0.15						30
V	1980	1989			0.40	0.67	1.95	0.36				66		
					0.33	0.20								30
VI	1990	1999			0.30	0.73	1.66	0.39				74		
						0.20	1.20							30
VII	2000	2010		0.20		0.27	1.40	0.40				64		

APPENDIX B: MODIFIED THOMPSON'S TAU TECHNIQUE

The procedure for evaluating the fitness of the data points is as follows (as defined by Cimbala 2011):

- the sample mean $\overline{x}$ and the sample standard deviation *S* are calculated in the usual fashion;
- for each data point, the absolute value of the deviation is calculated as $\delta_i = |d_i| = |x_i - \overline{x}|$;
- the data point most suspected as a possible outlier is the data point with the maximum value of δ_i;
- the value of the modified Thompson τ is calculated from the critical value of the student's t, and is therefore a function of the number of data point *n* in the sample;
- τ is obtained from the expression $\tau = \frac{t_{\alpha/2}*(n-1)}{\sqrt{n}\sqrt{n-2+t_{\alpha/2}{}^2}}$ where:
    - *n* is the number of data points
    - $t_{\alpha/2}$ is the critical student's t value, based on $\propto = 0.05$ and $df = n - 2$
- determine whether to keep or reject the suspected outlier by using the following simple rules:
    - if $\delta_i \leq \tau S$, keep the data point; it is not an outlier
    - if $\delta_i > \tau S$, reject the data point; it is an outlier

In this technique, only one suspected outlier was considered at a time – namely, the data point with the largest value of absolute deviation δ_i. If that data point is rejected as an outlier, it was removed and the procedure was repeated with the remaining data points until no more outliers are found.

APPENDIX C: CORRELATION AND REGRESSION COEFFICIENT

PEARSON PRODUCT-MOMENT CORRELATION COEFFICIENT (R)

Pearson's R measures the direction and strength of the linear relationship between the two variables, x and y, giving a value between +1 and −1, where 1 is total positive correlation, 0.0 is no correlation, and −1 is total negative correlation. The correlation measures the direction and strength of the linear relationship between two quantitative variables, in this case x and y for n individuals (Equation 3). Since correlation is not resistant, outliers which can greatly change the value of R were removed in the previous section.

Equation 3: Computational formula to calculate Pearson's R without computing deviation scores

$$R = \frac{\sum xy - \frac{\sum x \sum y}{n}}{\sqrt{\left(\sum x^2 - \frac{(\sum x)^2}{n}\right)}\sqrt{\left(\sum y^2 - \frac{(\sum y)^2}{n}\right)}}$$

REGRESSION COEFFICIENT (R^2)

The square of the sample correlation coefficient (R), typically denoted as R^2 is referred to as the regression coefficient or coefficient of termination, it summarizes the relationship between the two variables, x and y. If R^2 is 1.0, then given the value of one variable you can perfectly predict the value of the other variable. If R^2 is 0.0, then knowing either variable does not help you predict the other variable. In turn, the higher the R^2 value the more correlation there is between the two variables. However, extrapolation beyond the range of x value can be risky.

APPENDIX D: PROPOSED URBAN UNIT OF OBSERVATION FRAMEWORK (U2O) VARIABLES*

Geometric properties	Symbol	Unit	Range	Definition
Sky View Factor	ψ_{sky}	-	0-1	Mean value of the fraction of sky hemisphere visible from ground level
Aspect ratio	H/W	-	0-3^{+}	Mean height-to-width ratio of street canyons, consider length of streets as a weighting factor
Built area fraction	A_b/A_{tot} A_b : building plan area [m^2] A_{tot} : total ground area [m^2]	-	0-1	Ratio of building plan area to total ground area; fraction of ground surface with building cover
Unbuilt area fraction	1- A_b/A_{tot}	-	0-1	Ratio of unbuilt plan area to total ground area; fraction of ground surface without building cover
Impervious surface fraction	A_i	-	0-1	Ratio of unbuilt impervious plan area (paved, sealed) to total ground area
Pervious surface fraction	$A_p = (A_e + A_g + A_{H2O})$	-	0-1	Ratio of unbuilt impervious plan area (bare soil, green, water) to total ground area
	A_e : earth	-	0-1	Bare soil area
	A_g : green	-	0-1	Green area
	A_{H2O} : water	-	0-1	Water bodies area
Mean building compactness	l_c $l_c = V_b/ A_b$ [m^3/m^2] V_b : built volume [m^3]	m	-	Ratio of built volume (above terrain) to total building plan area
Built surface fraction	A_s/A_b A_s : total built surface area [m^2]	-	>1	Ratio of total built surface area (above terrain) of buildings (walls and roofs) to total built area
	A_W/A_b A_W : total wall area [m^2]	-	>1	Walls
	A_R/A_b $A_R = (A_{R,i} + A_{R,p})$ A_R : total roof area [m^2]	-	~1	Roofs
	$A_{R,i}/A_b$ $A_{R,i}$: total impervious roof area [m^2]	-	~1	Impervious roofs
	$A_{R,p}/A_b$ $A_{R,p}$: total pervious roof area [m^2]	-	~1	Pervious roofs
Mean sea level	h_{sl}	m	-	Average height above sea level

Surface/material properties	Symbol	Unit	Range	Definition
Reflectance/albedo	ρ_{sw}	-	0-1	Mean value of albedo (shortwave)
Thermal conductivity	$\lambda = (\lambda_i + \lambda_p)$	$W \cdot m^{-1} \cdot K^{-1}$	>0	The property of a material's ability to conduct heat
	λ_i : impervious surface	$W \cdot m^{-1} \cdot K^{-1}$	>0	Thermal conductivity of impervious surfaces
	λ_p : pervious surface	$W \cdot m^{-1} \cdot K^{-1}$	>0	Thermal conductivity of pervious surfaces
Specific heat capacity	$c = (c_i + c_p)$	$J \cdot kg^{-1} \cdot K^{-1}$	>0	The amount of heat required to change a unit mass of a material by one degree in temperature
	c_i : impervious surface	$J \cdot kg^{-1} \cdot K^{-1}$	>0	Specific heat capacity of impervious surfaces
	c_p : pervious surface	$J \cdot kg^{-1} \cdot K^{-1}$	>0	Specific heat capacity of pervious surfaces
Density	$\rho = (\rho_i + \rho_p)$	$kg \cdot m^{-3}$	>0	The mass density of a material is its mass per unit volume
	ρ_i : impervious surface	$kg \cdot m^{-3}$	>0	The mass density of impervious surfaces
	ρ_p : pervious surface	$kg \cdot m^{-3}$	>0	The mass density of pervious surfaces
Anthropogenic heat output	Q_F	$W \cdot m^{-2}$	>0	Mean annual heat flux density from fuel combustion and human activity (traffic, industry, heating and cooling of buildings, etc.)

**Excerpts taken from Document WP5-UHI-01_112012*